Ghana Journal of Geography

journal homepage: https://www.ajol.info/index.php/gjg/ https://journals.ug.edu.gh/index.php/gjg/

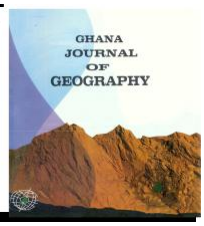

Modeling Land Surface Temperature Dynamics Using Biophysical and Environmental Drivers for Prescribed Fire Planning in Serengeti National Park

John Makunga [1,3*], Shadrack Sabai [2] & Fredrick Salukele [2]

[1]Ardhi University, School of Engineering and Environmental Studies, Department of Disaster Management Training, P. O. Box 35176, Dar es Salaam, Tanzania.

[2]Ardhi University, School of Engineering and Environmental Studies, Department of Environmental Engineering, P. O. Box 35176, Dar es Salaam, Tanzania.

[3]Ministry of Natural Resources and Tourism, Pasiansi Wildlife Training Institute, P.O. Box 1432, Mwanza, Tanzania.

article info

Article history:
Received 1st December 2024
Accepted 9th September 2025
Published 31st October 2025

Keywords:
Accuracy Assessment,
Land Surface Temperature,
Thermal Anomalies,
Prescribed Burning,
Biophysical and Environmental Drivers,
Wildfire.

abstract

Despite the extensive research on the factors that influence Land Surface Temperature (LST), the combined effects of vegetation structure, soil moisture, land cover dynamics, and fire activity on surface temperature regulation remain under-quantified across heterogeneous protected landscapes such as national parks. This study investigated the relationship between LST and multiple biophysical and environmental variables, including the Normalized Difference Vegetation Index (NDVI), burn severity (dNBR), soil moisture, and land cover, in Serengeti National Park, Tanzania, from 2001 to 2024, to support data-driven fire and habitat management strategies. Model evaluation metrics (R^2, MAE, RMSE, MAPE, BAE, and MBE) indicated high predictive performance, and residual analysis confirmed model validity and homoscedasticity. Grasslands overwhelmingly dominated the landscape (≈99%), while savannas expanded slightly and croplands declined after 2006. Burn severity analysis based on the dNBR classification revealed predominantly low to moderate severity, with limited areas of high severity concentrated in the western and central zones. Areas of higher burn severity corresponded to elevated LST, while unburned or lightly burned regions exhibited cooler temperatures and higher vegetation recovery potential. Soil moisture showed pronounced seasonal and interannual variability, with surface layers responding rapidly to rainfall, and deeper layers displaying greater stability and moisture retention. Peaks in 2006–2007, 2017–2018, and 2020–2021 coincided with wetter conditions, whereas declines occurred during prolonged dry periods. The results demonstrated a strong inverse relationship between NDVI and LST, highlighting vegetation's cooling effect and its role in post-fire recovery. The findings emphasize the importance of integrating LST and its biophysical predictors into fire and ecosystem management frameworks to enhance ecological resilience and guide adaptive, climate-informed decision-making in protected savanna landscapes.

Introduction

Prescribed fire, or early controlled burning, is the deliberate use of fire under specific weather conditions to manage forest and grassland fuels for ecological or risk-reduction goals (USDA, 2012). Prescribed burning is a key tool for wildfire risk management and ecosystem health, but it requires a suitable "burn window" for safe execution (Kupfer et al., 2020). Prescribed burns affect biophysical variables such as NDVI, vegetation structure and types, surface albedo, soil moisture, evapotranspiration, and Land Surface Temperature (LST). Fires raise surface air temperature by reducing latent heat flux through canopy damage and lower net radiation, as increased surface heating boosts longwave radiation emission (Li et al., 2017). Wildfires play vital ecological roles in grasslands and rangelands (Jolly et al. 2013). A wildfire is an uncontrolled fire in combustible vegetation, typically in rural areas (Sabuncu and Özener, 2018).

* Corresponding author.
E-mail address: jmakunga1@gmail.com (J. Makunga).

http://dx.doi.org/10.4314/gjg.v17i2.6

Fires shape savannah ecosystems by altering their vegetation structure and species composition (Takacs et al., 2021). More frequent or intense wildfires can promote invasive species (Reeves et al., 2018) and cause nitrogen loss in ungrazed grasslands, thereby reducing nitrogen availability and changing shoot-to-root ratios (Stavi, 2019). Fire also influences LST by lowering transpiration and increasing the Bowen ratio, reflecting changes in the land surface climate. These effects were measured using an eddy covariance system (Ren et al., 2022). The fire regime, characterized by the burned area, season, intensity, severity, and size, strongly influences biophysical variables and may feed back into climate warming through such effects (Zhao et al., 2021). Post-fire vegetation regrowth, reflected by changes in vegetation density, also impacts Land Surface Temperature (LST) owing to differences in emissivity between vegetation and bare ground. Thus, LST patterns can inform ecosystem recovery and guide post-fire management strategies (Vlassova et al., 2014).

Fire can enhance the productivity of perennial herbaceous plants by reducing competition for light and water and increasing nutrient availability. Burning biomass releases nitrogen, which becomes accessible to the regenerating vegetation (Bond and Keane, 2017). In Tanzania, areas such as the Serengeti National Park use prescribed burning to improve forage quality by converting biomass into more usable forms (Anderson et al., 2007). However, if poorly

managed, prescribed burns can hinder natural ecosystem processes and trigger uncontrolled fires (Strauch and Eby, 2012).

Frequent burning disrupts soil–vegetation–wildlife dynamics, reducing vegetation height and biomass, converting woody areas into grasslands, and promoting flammable or alien species (Scott et al., 2014; Masocha et al., 2011). It alters hydrology and increases erosion due to the soil degradation (Noske et al., 2024). Repeated fires may favor fire-adapted, less nutritious species and intensify grazing, enabling unpalatable or pioneer species to dominate the community (Anderson et al. 2007).

Fire effects depend on the fire regime, which is defined by the frequency, intensity, severity, seasonality, spatial extent, and individual fire events. Fire regimes reflect the interactions among climate, fuel, and ignition patterns (Bond and Keane, 2017). In the savannas, fire regimes strongly influence vegetation, particularly the tree cover. Late dry-season (LDS) fires are typically more harmful to trees than early dry-season (EDS) fires, as shown by long-term experiments inspired by Aubréville's early work (Ryan and Williams, 2011; Higgins et al., 2007; Sankaran et al., 2004; Laris, 2016).

Effective fire management is, therefore, essential for protecting biodiversity, regardless of the fire type or method. Advances in remote sensing have aided fire risk mapping, fuel load assessment, active fire detection, burn severity, LST analysis, and post-fire recovery monitoring (Szpakowski and Jensen, 2019). The impact and intensity of fires depend on fuel loads and vegetation composition (Sriramamurthy et al., 2022). Land Surface Temperature (LST) is crucial for fire susceptibility mapping, as it reflects the thermal conditions that affect vegetation flammability. Higher LST often indicates drier vegetation and a greater ignition risk (Jodhani et al., 2024). In wildfire studies, LST acts as both a pre-fire indicator of dryness and a post-fire marker of environmental change (Stoyanova et al. 2022).

Temperature affects fuel moisture and ignition potential, making it vital for assessing fire-prone conditions in forests. Fire reduces transpiration, thereby altering LST patterns after disturbance. Precipitation also influences fuel moisture and the risk of wildfires. Adequate rainfall lowers vegetation dryness and ignition risk, whereas drought increases susceptibility (Jodhani et al., 2024). Heavy rain can boost vegetation growth, increasing fuel loads and future fire risk. With the intensification of climate extremes, large wildfires in semi-arid regions are expected to increase, potentially changing the distribution of fire-sensitive plants (Donnell et al., 2011).

Fire occurrence depends on the moisture content in dead and live biomass, with antecedent climate and weather influencing burn timing. The warm and dry period required for ignition is shaped by vegetation characteristics (Bond and Keane, 2017). Fire frequency often increases during dry, hot El Niño phases, whereas cool, wet summers suppress fires, linking fire occurrence and severity to precipitation and temperature anomalies. Major fire years typically follow droughts that occur after wet, cool springs and summers (Donnell et al., 2011). Probability analyses have shown a strong positive correlation between wildfire occurrence and daily temperatures in dry months, with fire likelihood rising sharply on hotter days (Gutierrez et al., 2021).

Effective planning for prescribed burning in grassland and forest ecosystems requires a consideration of regional and seasonal variations in temperature, precipitation, and fire risk, as well as some other social and environmental factors. Integrating Earth Observation technologies can improve fire hazard models by assessing live fuel quality (Sivakumar et al., 2024). Spectral indices, such as NDVI and dNDVI, offer insights into vegetation health and post-fire recovery, especially when combined with temperature and precipitation data. A holistic understanding of fire drivers and their impacts is essential for the sustainable management of terrestrial and protected ecosystems (Jodhani et al., 2024).

Climate models and in situ measurements are key tools for assessing the climatic impacts of forest change according to (Bonan, 2008). LST is often analyzed alongside NDVI or similar indices for a more integrated understanding (Julien et al. 2011). Models simulate the effects of forest cover changes, such as deforestation, on climate variables, whereas in situ data help in validating these simulations (Li et al., 2022). As forest disturbances influence land biophysics and local climate, their effects on LST are challenging to isolate using only pre- and post-disturbance data. Comparing nearby undisturbed sites helps to control for background climate variability (Li et al., 2022).

Vegetation plays a crucial role in regulating Land Surface Temperature (LST) through processes such as evapotranspiration and canopy shading, which significantly lower surface temperatures and improve microclimatic conditions (Oliveira et al., 2011). As a key indicator of surface energy balance, LST effectively represents the water–heat exchange processes at the Earth's surface and provides valuable insights into environmental change (Bindajam et al., 2020). However, the long-term magnitude and spatial variability of vegetation-driven LST regulation remain poorly quantified across diverse and heterogeneous landscapes, particularly within protected areas such as national parks. This gap limits our understanding of vegetation–climate interactions and constrains the development of evidence-based fire and ecosystem management strategies that account for the dynamic interactions between vegetation and climate. Addressing this knowledge gap requires integrated assessments that link vegetation structure, density, and surface thermal characteristics to ecological resilience and fire behavior. Consequently, accurate and spatially explicit analyses of vegetation and heat dynamics are essential to guide effective prescribed burning practices and promote sustainable ecosystem management.

To address these challenges, this study examined the spatial and temporal relationships between multiple variables, including vegetation density (NDVI), vegetation types, vegetation recovery, soil moisture, precipitation, and burn severity, and Land Surface Temperature (LST), to quantify the thermal regulation effects of vegetation. By linking variations in these predictors with LST changes, the analysis informs the strategic planning of prescribed burns, identifying optimal zones and timing based on key environmental and climatic factors. This approach enhances fire safety, minimizes ecological risks, and strengthens ecosystem resilience. Overall, these findings contribute to a deeper understanding of vegetation–climate–fire interactions, thereby supporting more effective and adaptive land management in fire-prone regions.

Material and Methods

Designated as a game reserve in 1940 and granted full protection in 1948, Serengeti National Park (SENAPA) spans 14,763 km², making it Tanzania's third-largest park after Nyerere (30,893 km²) and Ruaha (20,226 km²) (Kideghesho, 2010; Nyerere National Park, 2024; Serengeti National Park, 2020). The greater Serengeti ecosystem extends over ~25,000 km² in northern Tanzania (Kideghesho, 2010), between 1°50′–3°00′ S and 34°00′–35°50′ E. It is bordered by the Maswa, Kijereshi, Loliondo, and Ikorongo–Grumeti reserves, the Ngorongoro Conservation Area, and Kenya's Maasai-Mara Reserve (Nkwabi and Kavana, 2022). In 1981, SENAPA was designated a UNESCO World Heritage Site and included in the Serengeti–Ngorongoro Biosphere Reserve (Serengeti National Park, 2024; Nsemwa, 2020; Botha, 2021).

Soil surveys in the Serengeti woodlands have revealed that volcanic deposits significantly influence soil chemistry (Tiger, 1982). The park's bimodal rainfall pattern, driven by the Intertropical Convergence Zone, features a dry season from June to September and a wet season from October to May, with peak rains in November–December (vuli) and March–May (masika) (Sinclair et al., 2008; Huang et al., 2021; Mahony et al., 2020). Annual rainfall averages 900–1,000 mm (Serengeti National Park Safaris, 2022), with temperatures rarely exceeding 37 °C or falling below 13 °C. Vegetation varies from open grasslands to hilly woodlands and savannahs, contributing to the region's ecological diversity.

Serengeti National Park, located within a global Endemic Bird Area, supports over 500 bird species (IUCN and UNEP-WCMC, 2017). Frequent fires have increased grass and shrub species richness but have also encouraged invasive plants and fire-adapted, low-nutrition species (Ayron et al., 2012; Masocha et al., 2011; Anderson et al., 2007). Given threats such as poaching, disease, and climate change, managers require species-specific knowledge of fire responses to guide effective prescribed-burning strategies (van Wilgen et al., 2003).

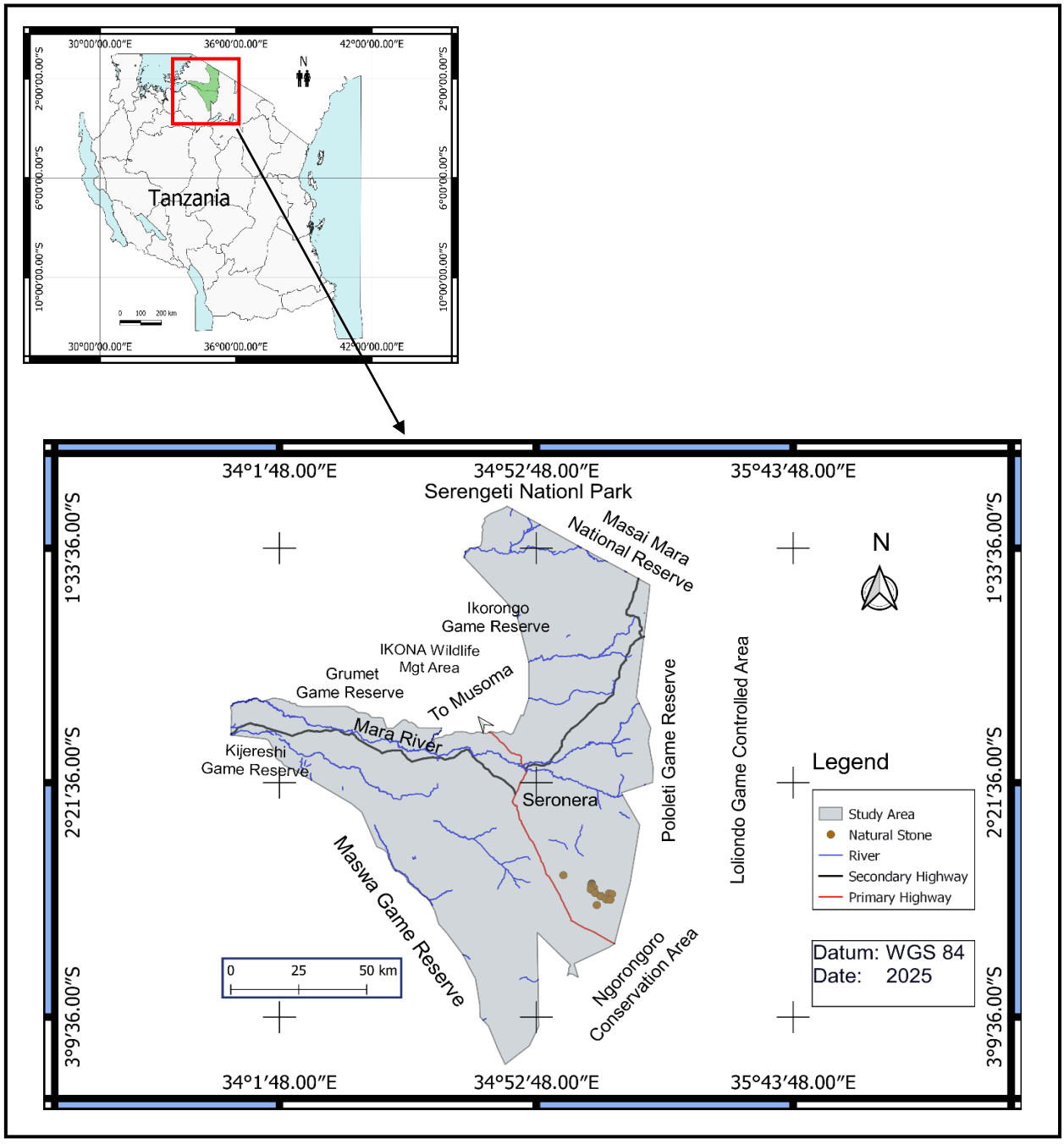

Figure 1. Map of Serengeti National Park

Land Surface Temperature (LST) was derived from the MOD11A2 Terra product using the standard MODIS split-window algorithm, with atmospheric corrections applied. Processing was performed in Google Earth Engine (GEE) using the following predictor bands: NDVI_ Recovery, Soil Moisture Mean, Shannon, Burn Severity, LC_Type1, and a constant (Const) band. Vegetation cover and recovery were quantified using NDVI from the MOD13A1 MODIS product (500 m resolution), with values ranging from (–1) to (1). Vegetation heterogeneity was further characterized using Shannon diversity indices. The Fast, kernel-free Shannon Diversity Index (SDI) was employed to quantify landscape heterogeneity, avoiding the use of traditional 3×3-pixel kernels or other neighborhood-based methods. This approach enables rapid computation of landscape-level diversity over large areas while minimizing memory and processing demands. This approach provides robust area of interest-wide Shannon diversity values, making it ideal for temporal trend analysis and multi-year comparisons.

Land cover was assessed using the MODIS LC_Type1 product (IGBP scheme) at 500 m resolution, the categorical land cover classification from MODIS MCD12Q1, to capture spatial variability. The land cover dataset was processed to quantify the spatial extent of different vegetation types, including grasslands, savannas, croplands, wetlands, and barren land. These data were subsequently used to characterize vegetation composition and heterogeneity across the park and incorporated as predictor variables in models examining Land Surface Temperature (LST) patterns. To capture fine-scale variability, the methodology allows for integration of higher-resolution land cover datasets or additional vegetation metrics where available.

Soil moisture (hydrological modeling dataset) analysis was conducted using the NASA FLDAS (Famine Early Warning Systems Network Land Data Assimilation System) NOAH01 dataset, which provides global soil moisture data across multiple depths. While precipitation patterns were incorporated to capture seasonal and interannual variability in surface moisture. The dataset

was filtered by spatial extent (AOI) and temporal range (2001–2024), and relevant soil moisture bands were selected for three depth intervals: 0–10 cm, 10–40 cm, and 40–100 cm. Each image in the collection was clipped to the area of interest, and a mean soil moisture value was computed across all depths using pixel-wise averaging. Visualization was performed using false-color maps and time-series charts to examine temporal dynamics.

Burn severity was quantified using the differenced Normalized Burn Ratio (dNBR) derived from pre- and post-fire Sentinel-2 imagery. Additionally, MODIS (MOD09A1) data were used to compute annual dNBR values, providing an independent, coarser-resolution dataset for comparison and multi-year fire trend assessment. Together, these predictor variables including vegetation recovery (NDVI), land cover type, soil moisture, precipitation, and burn severity were integrated to model and predict Land Surface Temperature (LST). This integration enabled the detection of thermal anomalies, evaluation of post-fire vegetation recovery, and the development of adaptive fire management strategies such as prescribed burning and high-risk area assessment.

A random sample of 5,000 pixels was initially extracted from the predictor stack over the study area. Valid-pixel counts (n = 52,637) were used to evaluate LST data coverage, and a stratified random sample of 4,988 pixels was selected for model training and validation. Random samples were spatially dispersed to minimize spatial autocorrelation in the regression analysis. Only valid, non-masked LST pixels with complete predictor information were included, ensuring the exclusion of clouds, water bodies, and sensor artifacts. To simulate natural variability present in satellite-derived LST (e.g., sensor error, atmospheric disturbance, viewing geometry, processing uncertainty), small random noise was added to the model predictions. This prevents artificially smooth outputs and produces realistic scatter and residual distributions for meaningful accuracy assessment.

Noise may be added to remotely sensed data during different stages of data acquisition or processing, from the moment the data are captured by the sensor until their atmospheric and topographic correction, orthorectification, or co-registration (Petrou et al., 2014). In satellite image classification, the data obtained from the satellite sensors may be affected by atmospheric noise resulting from the obstruction of the light reflected by targets on the Earth's surface by a variety of phenomena, including aerosols and clouds in the atmosphere as well as changing illumination patterns and the angle at which the satellite views the ground at any given time (Simonetti, et al., 2014).

LST modeling employed a Multiple Linear Regression (MLR) framework, a supervised regression approach, to quantify the relationships between LST and five key biophysical predictors (explanatory variables): NDVI recovery, mean soil moisture, Shannon diversity index, burn severity (dNBR), and land cover type (LC_Type1). Multiple Linear Regression (MLR) assumes that the dependent variable (LST) varies linearly with the independent predictors, producing coefficients that quantify the relative impact of each factor or predictor variable on LST. (Jia *et al*., 2023). This model was used to estimate the combined effects of these variables on spatial and temporal variations in LST across the study area.

Pre-processing workflow for LST involved top-of-atmosphere (TOA) correction, cloud and shadow masking using QA flags, clipping to the area of interest (AOI), and temporal gap-filling for cloud-covered regions using the mean of the cloud-free pixels across multiple acquisition dates, the approach, which has been adopted by Lee et al. (2025). Pre-fire and post-fire LST maps were classified into hotter, cooler, and unchanged zones to assess fire-induced thermal variations. All datasets were reprojected, resampled, and spatially aligned to ensure accurate correlations between LST and predictor variables. Seasonal median composites were applied to reduce atmospheric and illumination noise, resulting in clean, continuous datasets suitable for LST trend analysis, regression modeling, and prediction of prescribed burn effects.

Residuals between observed and predicted values were squared to compute the Sum of Squared Residuals (SSR), while the Total Sum of Squares (SST) was derived from the observed mean to calculate the Coefficient of Determination (R^2). Accuracy assessment was used to evaluate LST classification, while predictive accuracy was measured using the Mean Bias Error (MBE), Bias-Adjustment Error (BAE), Mean Absolute Error (MAE), Root Mean Square Error (RMSE), Mean Absolute Percentage Error (MAPE), and Coefficient of Determination (R^2) metrics. The model performance was assessed for a long term from 2001 to 2024, providing temporal insight into its reliability. LST validation typically involves four methods: ground-based validation comparing radiance measurements, scene-based inter-comparison with legacy satellite products, radiance-based validation using radiative transfer models, and time series comparisons to identify sensor issues. Reference LST datasets remain essential (Guillevic et al., 2018).

For climate studies, LST products require a minimum 20-year time series, ideally exceeding 30 years (Guillevic et al., 2018). Validation typically quantifies the bias and deviation metrics (Schneider et al., 2012). The bias, standard deviation, and RMSE between the Landsat-derived and in situ LST across land types were calculated (Duan et al., 2021; Schneider et al., 2012). Cloud contamination limits LST to clear-sky observations, causing clear-sky biases in the data (Equations 14 and 15), making clouds a major source of retrieval bias (Pan et al., 2024). A positive bias indicates satellite LST overestimation, whereas a negative bias indicates underestimation (Agbor and Makinde, 2018; Schneider et al., 2012). Mean Bias Error (MBE) assesses the systematic deviation in the predicted LST, which is important for burned area estimates to detect over- or underestimation (Erick et al., 2017).

The Multiple Linear Regression (MLR) model used to predict and validate Land Surface Temperature (LST) is expressed as:

$$\text{Land Surface Temperature (LST)} = \beta_0 + \beta_1 \times \text{NDVI} + \beta_2 \times \text{VegDiversity} + \beta_3 \times \text{VegTypes} + \beta_4 \times \text{SoilMoisture} + \beta_5 \times \text{BurnSeverity} + \epsilon \quad (1)$$

Where;

LST = the dependent variable (Land Surface Temperature)

NDVI (vegetation recovery) was an independent predictor variable

VegDiversity = Vegetation diversity, represented by Shannon diversity index

VegTypes = categorical or continuous variable representing vegetation types (e.g., grasslands, savannas, wetlands)

SoilMoisture = independent predictor representing average soil moisture in relevant soil layers

BurnSeverity = burn intensity, e.g., dNBR

β_0 = intercept (the constant term)

β_1, β_2, β_3, β_4, β_5 = regression coefficients showing the effect of NDVI (vegetation recovery), vegetation diversity (Shannon index), vegetation types (Land Cover), soil moisture and burn severity on LST

ϵ = the error term (the residual or unexplained part of the dependent variable that is not accounted for or explained by the predictors)

Shannon diversity formula (Ulfah *et al*., 2019; Shannon and Wiener, 1949)

$$H = -\sum_i pi \, \ln(pi) \quad (2)$$

Where;

H = Shannon diversity index

pi = proportion of pixels belonging to the *i*-th land cover class in the neighborhood

i = index for each land cover class (from 1 to n)

n = total number of classes in the neighborhood

$$\text{Mean Absolute Error (MAE)} = \frac{1}{n}\sum_{i=1}^{n}|y_i - \overline{y_i}| \quad (3)$$

$$\text{Root Mean Squared Error (RMSE)} = \sqrt{\frac{1}{n}\sum_{i=1}^{n}|y_i - \bar{y}|} \quad (4)$$

$$\text{Coefficient of Determination } (R^2) = 1 - \frac{\sum_{i=1}^{n}(Y_{observed\_i} - Y_{predicted\_i})^2}{(Y_{observed\_i} - \overline{Y}_{observed})^2} \quad (5)$$

Where;

For both MAE and RMSE, and for R^2 (Mestre-Runge *et al*., 2023).

R^2 = Coefficient of determination or Kappa Coefficient

n = the number of observations (data points) available for the analysis

y_i = the actual or observed value (historical fire points in study areas)

$\overline{y_i}$ = the predicted value

$Y_{observed\_i}$ = the observed LST value for the *i*-th observation

$Y_{predicted\_i}$ = the predicted LST value from the validation model for the *i*-th observation

$\overline{Y}_{observed}$ = the mean of the observed LST values

The numerator is the Sum of Squared Residuals (SSR)

The denominator is the Total Sum of Squares (SST), i.e. the sum of squared deviations from the mean

$$\text{Mean Bias Error (MBE)} = \frac{1}{n}\sum_{i=1}^{n}(LST_{predicted} - LST_{obsrved}) \quad (6)$$

Where;

LST_{sat} = Satellite-derived LST

LST_{ref} = Observation of a given reference LST (ground truth data), which is assumed to be closer to the true value (Schneider *et al.*, 2012).

The residual (bias) for the *i*-th observation (i.e., for each pixel or sample, is given by the formula:

$$e_i = y_i - \hat{y}_i \quad (7)$$

Where;

e_i = residual for the *i*-th observation (i.e., for each pixel or sample)

y_i = observed (actual) LST values

$\hat{y}_i$ = predicted (fitted) LST value from the regression model

Interpretation:

If $e_i > 0$: the model underestimated the observed LST (i.e. predicted too low)

If $e_i < 0$: the model overestimated the observed LST (i.e. predicted too high)

If e_i = 0: the model has no systematic bias

Ideally, residuals (bias) should average around zero with no systematic pattern as revealed by Gunashree (2024).

$$\text{Bias} - \text{Adjusted Error (BAE)} = \frac{1}{n}\sum_{i=1}^{n}\left|(P_i - \hat{P}) - (Q_i - \hat{Q})\right| \quad (8)$$

Where;

P_i = Predicted value

P = Observed (actual) value

Q_i = Mean of predicted values

Q = Mean of observed values

n = Number of observations

BAE is equivalent to the MAE of bias-corrected residuals (see MAE formula)

The term $(P_i - \hat{P}) - (Q_i - \hat{Q})$ removes the average bias between predictions and observations before computing the absolute error. The Error adjusted for bias is equal to the deviation from mean prediction minus deviation from mean observation.

$$\text{Mean Absolute Percentage Error (MAPE)} = \frac{1}{n}\sum_{i=1}^{n}\left|\frac{Y_i - \hat{Y}_i}{Y_i}\right| \times 100 \quad (9)$$

Where;

Y_i = Observed value (actual value)

$\hat{Y}$ = Predicted value (model's prediction)

n = Total number of observations

The analysis of Land Surface Temperature (LST) was conducted following a structured workflow, as outlined in the flowchart (Fig. 2), which delineates all essential steps involved in the process.

Land Surface Temperature (LST)

$$\text{Land Surface Temperature (LST)} = \frac{T_B}{1 + (\lambda \cdot T_B/\rho)\cdot ln\varepsilon} \quad (10)$$

Where;

LST = Land Surface Temperature (in Kelvin)

T_B = At-sensor brightness temperature (in Kelvin)

λ = Wavelength of emitted radiance (typically around 10.895 μm for Landsat 8 Band 10)

ε = Surface emissivity (unitless, varies by land cover type)

$\rho = \frac{hc}{\sigma} \approx 1.438 \times 10^{-2}$ m·K

With m·K = metres·Kelvin, h = Planck's constant, c = speed of light, σ = Boltzmann constant

$$\text{Delta LST (dLST)} = LST_{post} - LST_{pre} \quad (11)$$

Where:

dLST = Change in Land Surface Temperature (in °C or K)

LST_{post} = LST at the later date (e.g., after fire period)

LST_{pre} = LST at the earlier date (e.g., before fire period)

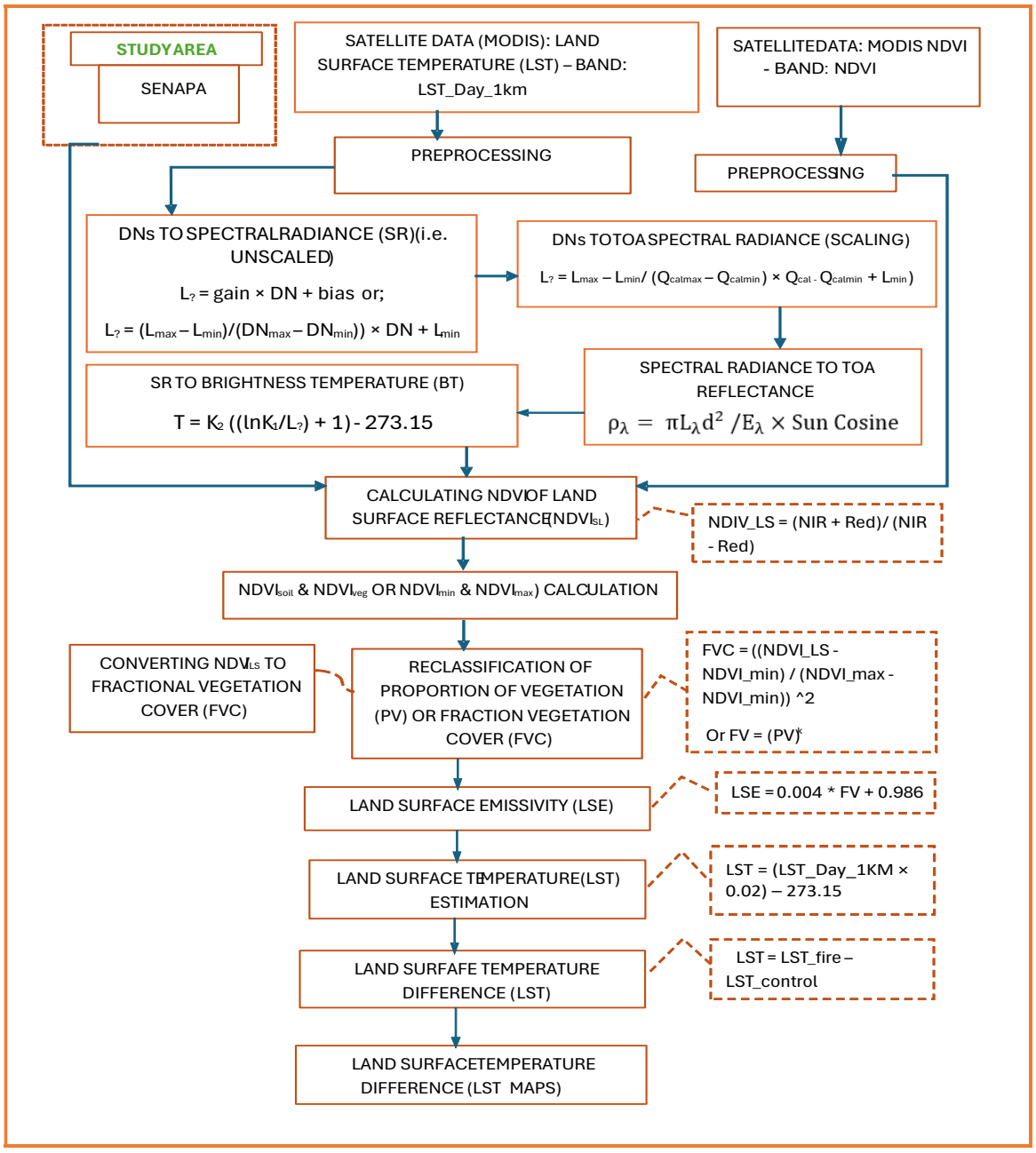

Figure 2. Flowchart of Land Surface Temperature

Results and Discussion

Predictor Contributions and Performance of the LST Regression Model

The multiple linear regression model quantified the influence of five environmental predictors on Land Surface Temperature (LST): NDVI recovery, soil moisture, Shannon diversity, burn severity (dNBR), and land cover type (LC_Type1). The model intercept was 35.26 °C, representing baseline LST when all predictors are zero. LST decreased with increasing NDVI recovery (–0.97), soil moisture (–33.63), and Shannon diversity (–1.35), indicating that areas with greater vegetation regrowth, higher surface moisture, and more diverse landscapes are cooler. In contrast, burn severity (+2.73) and land cover type (+0.52) had positive effects, reflecting warmer conditions in burned or sparsely vegetated areas. These results highlight vegetation recovery, soil moisture, and fire disturbance as key drivers of LST variability, with implications for thermal monitoring and adaptive fire management.

The regression results align with ecological and biophysical expectations that vegetation regrowth and soil moisture enhance evapotranspiration and surface shading, leading to reduced LST. Conversely, fire-affected areas with exposed soil or reduced canopy cover exhibit elevated temperatures. The moderate positive influence of land cover likely reflects surface heterogeneity and differences in emissivity among land-cover types. Overall, the model demonstrates that integrating post-fire vegetation, moisture, and structural diversity metrics provides a reasonable prediction of spatial LST variation across the Serengeti National Park landscape.

The multiple linear regression model linking long-term mean Land Surface Temperature (LST) (averaged over 2002–2024) with environmental and biophysical predictors: NDVI recovery, soil moisture, Shannon diversity, burn severity (dNBR), and land cover type (LC_Type1), achieved moderate predictive performance with an R^2 (Coefficient of Determination) of 0.35, indicating that approximately 35% of the spatial variation in LST across the

Serengeti ecosystem was captured or explained by the selected variables in the regression model, leaving 65% of variability unexplained.

Accuracy Assessment

Quantitatively, the model achieved a Root Mean Square Error (RMSE) of 0.99 °C, reflecting the average magnitude of residuals, and a Mean Absolute Error (MAE) of 0.78 °C, indicating strong agreement between observed and predicted LST values. The Mean Absolute Percentage Error (MAPE) of 2.36% confirms high relative accuracy across the dataset. Additionally, the Mean Bias Error (MBE) is effectively zero (3.55×10^{-14} °C), demonstrating that there is no systematic over- or underestimation. The Bias-Adjusted Error (BAE) of 0.78 °C confirms that prediction errors remain small even after accounting for any residual bias. Overall, both the visual residual plots and statistical metrics indicate that the model provides accurate LST predictions, with residuals randomly distributed and minimal bias, supporting the model's reliability for temporal and spatial LST analysis. The regression metrics were used to assess the agreement between observed and predicted LST values across years. Together, these metrics indicate that the regression model provides a reliable first-order approximation of LST variability, with vegetation recovery, soil moisture, and fire disturbance identified as key drivers.

The relationship between predicted and observed Land Surface Temperature (LST) for the years 2001, 2010, 2020, and 2024 (Figs. 3–10) showed positive slopes close to 1 in all cases, indicating a strong linear agreement between model predictions and observed values. The coefficients of determination (R^2) ranged from 0.2145 in 2020 to 0.3576 in 2024, suggesting that the model explained approximately 21 % to 36 % of the observed LST variation, while the remaining variation (about 64 % to 79 %) was not captured by the predictor variables.

Residual Analysis

The residual analysis (Figures 4, 6, 8, and 10) illustrates the distribution of differences between observed and predicted Land Surface Temperature (LST) across the study years (2001, 2010, 2020, and 2024). Residuals were generally symmetrically distributed around zero, with no apparent systematic trend relative to the predicted LST values, indicating that the model does not consistently over- or under-predict temperatures. The mean residuals for the study years were very close to zero, as computed from the datasets using the Mean Bias Error (Equation 6), indicating that the model predictions were essentially unbiased across all years.

This suggests that the residuals are randomly distributed, confirming that key model assumptions, such as linearity and homoscedasticity (i.e., constant variance of residuals across predicted values), were largely satisfied. The symmetric distribution of residuals around zero further supports the model's precision and unbiased nature. The linear fit of residuals versus predicted LST is effectively flat, with slopes near zero and R^2 values close to zero, further confirming the absence of bias in the model predictions.

The positive slopes (close to 1) in the predicted vs. observed LST plots indicate that, on average, for every 1 °C increase in observed LST, the model predicted approximately 1 °C, demonstrating strong agreement. The small intercepts, ranging between 0.21 °C (2020) and 0.36 °C (2024), suggest minimal systematic bias. However, the slightly negative slopes in the residual plots imply that the model tended to underpredict LST at higher values and overpredict at lower values, though the effect was minor given the near-zero slope magnitudes.

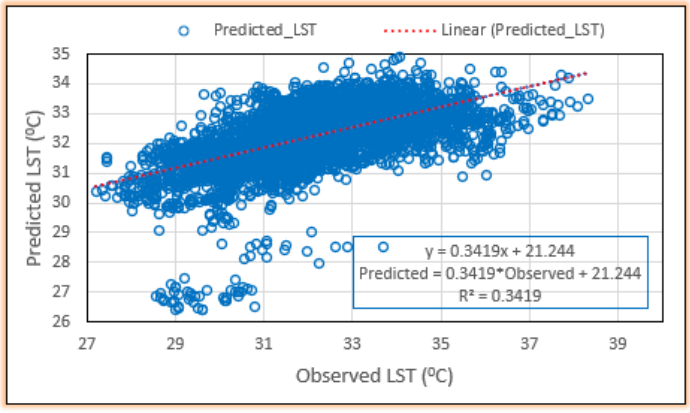

Figure 3. Model prediction accuracy for LST in 2001 (n = 4,988)

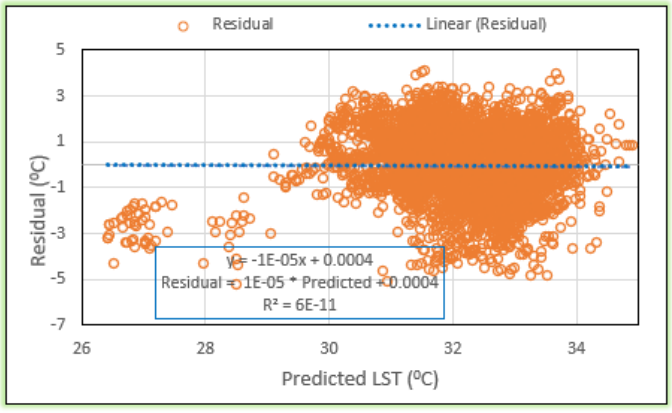

Figure 4. Residual analysis of LST predictions in 2001 (n = 4,988)

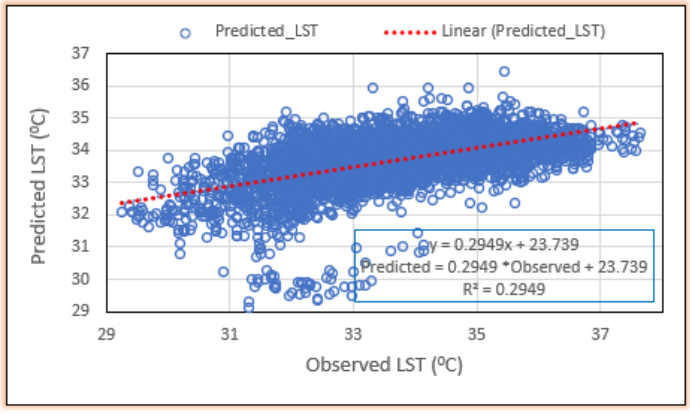

Figure 5. Model prediction accuracy for LST in 2010 (n = 4,988)

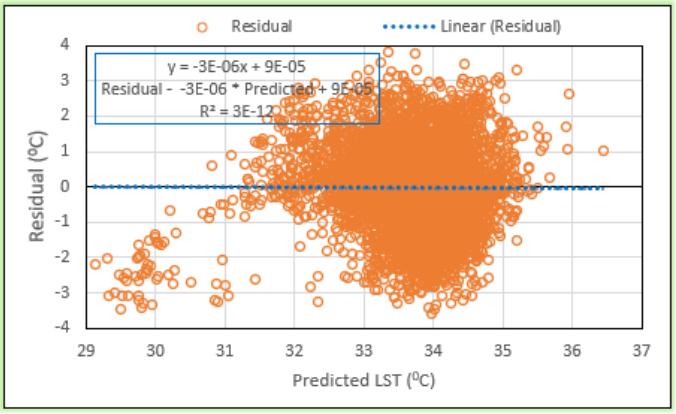

Figure 6. Residual analysis of LST predictions in 2010 (n = 4,988)

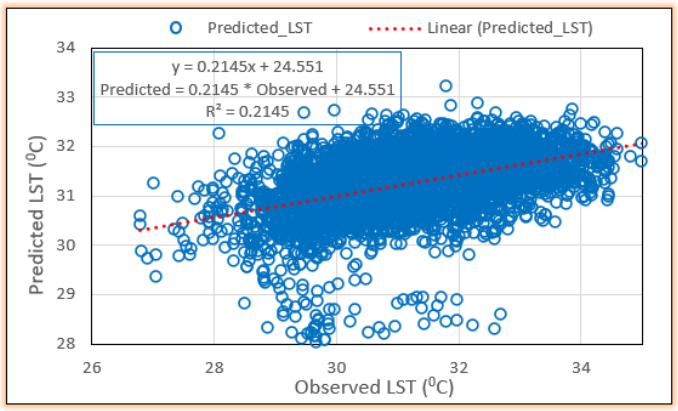

Figure 7. Model prediction accuracy for LST in 2020 (n = 4,988)

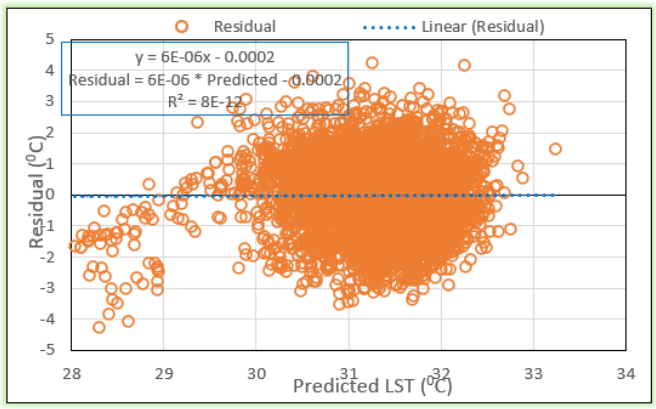

Figure 8. Residual analysis of LST predictions in 2020 (n = 4,988)

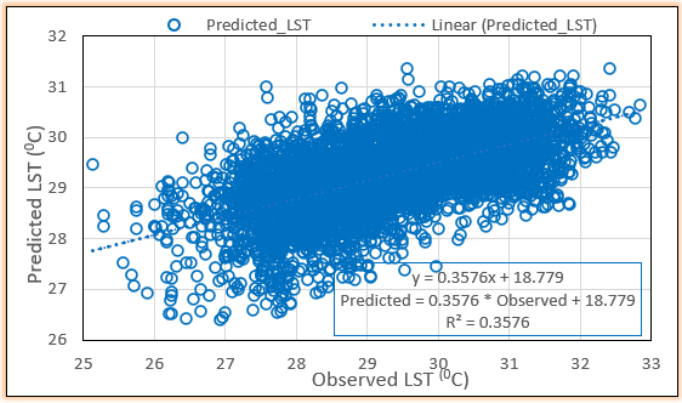

Figure 9. Model prediction accuracy for LST in 2024 (n = 4,988)

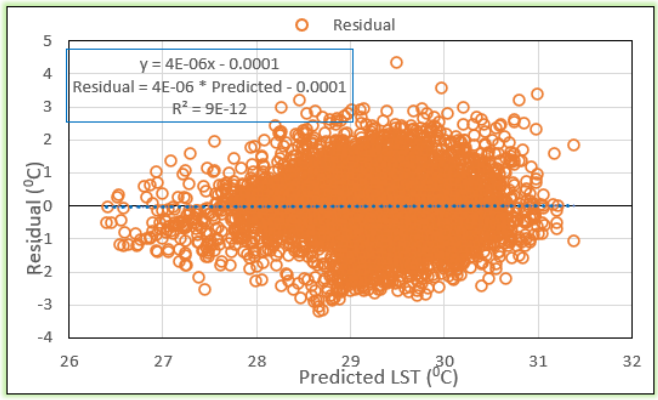

Figure 10. Residual analysis of LST predictions in 2024 (n = 4,988)

The Pearson correlation coefficient between observed and predicted Land Surface Temperature (LST) values, computed using the sampled points, was r = 0.24 ($p < 0.001$). This indicates a weak but, statistically significant positive linear relationship between the observed and modeled LST values. Although the correlation is low, the very small p-value ($\approx 1.05 \times 10^{-65}$) confirms that the relationship is not due to random chance. The relatively weak correlation suggests that while the regression model captures some of the variation in LST, there remain considerable unexplained differences between predicted and observed values. These discrepancies could stem from the spatial heterogeneity, sensor noise, simplified predictor variables, or nonlinear interactions not fully accounted for in the model.

Residual analysis was performed to assess whether the residuals were randomly distributed around zero and to verify that model assumptions, such as linearity and homoscedasticity, were satisfied. The presence of systematic patterns in the residuals would indicate a potential model misspecification. The residuals, representing the difference between predicted and observed LST values for 2024, ranged from –0.67 to –0.96 °C among the first ten sampled points. All residuals were negative, indicating that the model consistently underestimated LST at these locations rather than overestimating it. This corresponds to an underestimation bias of approximately 0.8 °C, which is acceptable and well within normal limits for LST reconstruction. Across all years, the first ten residuals for the validation points similarly fell within a narrow range, demonstrating minimal variance in the prediction errors.

The moderate spread of residual magnitudes suggests variability in model performance across different areas, likely reflecting spatial heterogeneity in surface characteristics or limitations in predictor sensitivity to local temperature variations. While the overall metrics ($R^2 = 0.35$, RMSE = 0.99 °C, MAE = 0.78 °C, MBE ≈ 0) indicate that the model is unbiased and reasonably accurate at the regional scale, the presence of small but systematic positive residuals in some locations, coupled with the moderate explanatory power (Coefficient of Determination), suggests that the local LST variability remains partially unaccounted for. These findings highlight the potential for improved performance through the inclusion of additional or more complex environmental predictors or by employing alternative modeling approaches that better capture spatial heterogeneity.

It has been theorized that people generally make accurate estimations of a target variable (TV) when the actual value of the situational variable (SV) is near its central tendency, but that they are less sensitive to variations in the SV. Many prediction biases arise because individuals fail to account for changes in situational variables, and consequently, in the corresponding target variables. Positive bias occurs when predictions are systematically overestimated on average, whereas negative bias occurs when predictions are systematically underestimated (Yang et al., 2021).

Land Surface Temperature

The results indicated that pre-fire Land Surface Temperature (LST) ranged from 24.52–35.69°C in 2001, 25.96–34.97°C in 2010, 24.06–31.84°C in 2020, and 23.45–30.92°C in 2024 (Fig. 11). In contrast, post-fire LST values ranged from 27.81°C to 42.76°C in 2001, 29.31°C to 41.65°C in 2010, 27.95°C to 40.31°C in 2020, and 25.44°C to 37.28°C in 2024 (Fig. 11). The overall, minimum temperature during the pre-fire period was 23.45°C, whereas the maximum was 35.69°C. During the post-fire period, LST generally ranged from 25.44°C to 42.76°C. In 2024, the pre-fire map (Fig. 11) showed that many areas in the southwest, east, and northeast of the park experienced lower temperatures. Most regions in the west, central, north, and south exhibited medium temperatures, with no areas reaching high temperatures during this period. Conversely, in the post-fire period of 2020, the park was predominantly characterized by low to medium temperatures, although the western and central parts were notably hotter than other regions, which mostly experienced medium temperatures.

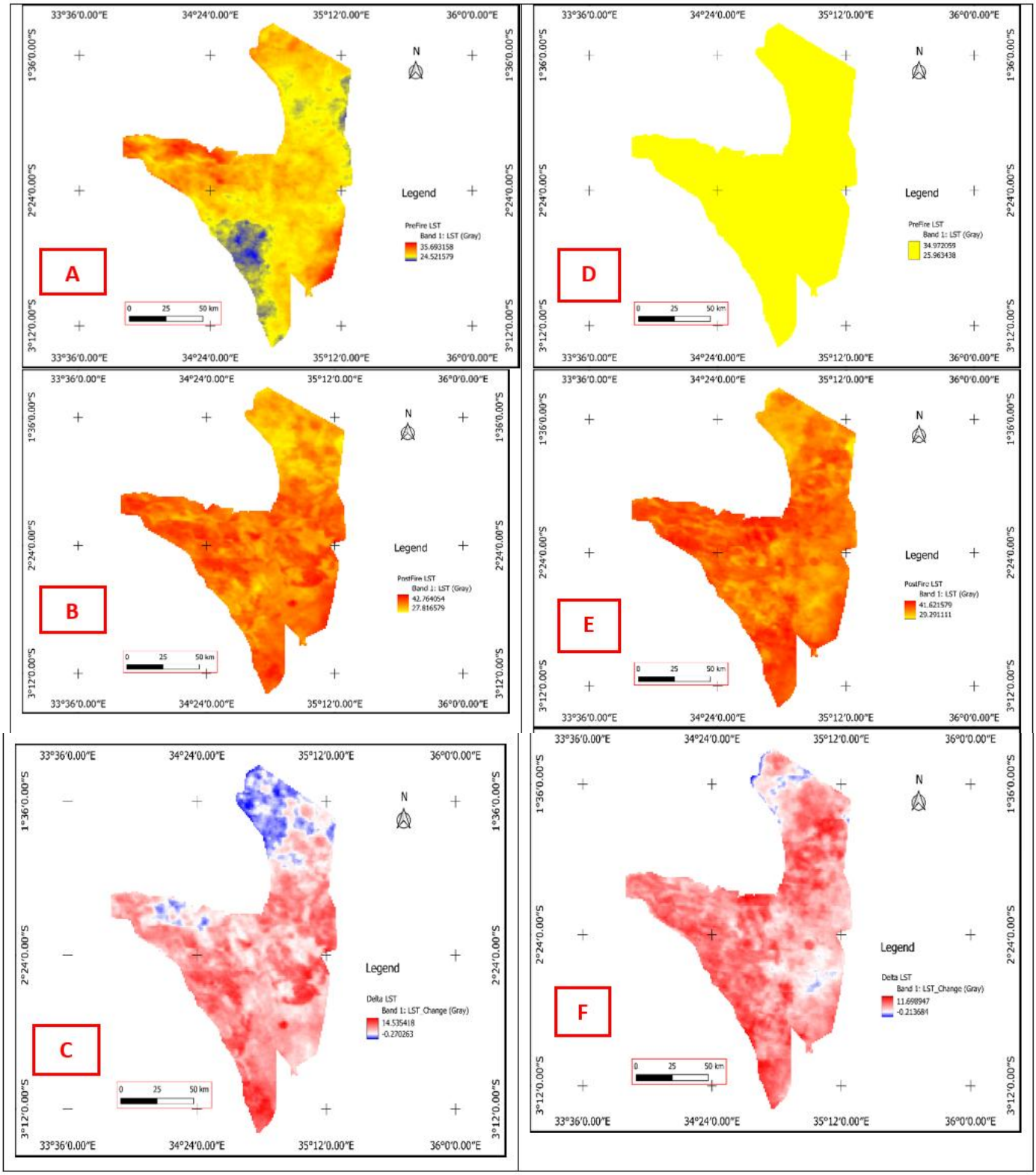
A
33°36'0.00"E
34°24'0.00"E
35°12'0.00"E
36°0'0.00"E
1°36'0.00"S
2°24'0.00"S
3°12'0.00"S
N
Legend
PreFire LST
Band 1: LST (Gray)
35.693158
24.521579
0 25 50 km
D
Legend
PreFire LST
Band 1: LST (Gray)
34.972059
25.963438
0 25 50 km
B
Legend
PostFire LST
Band 1: LST (Gray)
42.764054
27.816579
0 25 50 km
E
Legend
PostFire LST
Band 1: LST (Gray)
41.621579
29.291111
0 25 50 km
C
Legend
Delta LST
Band 1: LST_Change (Gray)
14.535418
-0.270263
0 25 50 km
F
Legend
Delta LST
Band 1: LST_Change (Gray)
11.698947
-0.213684
0 25 50 km

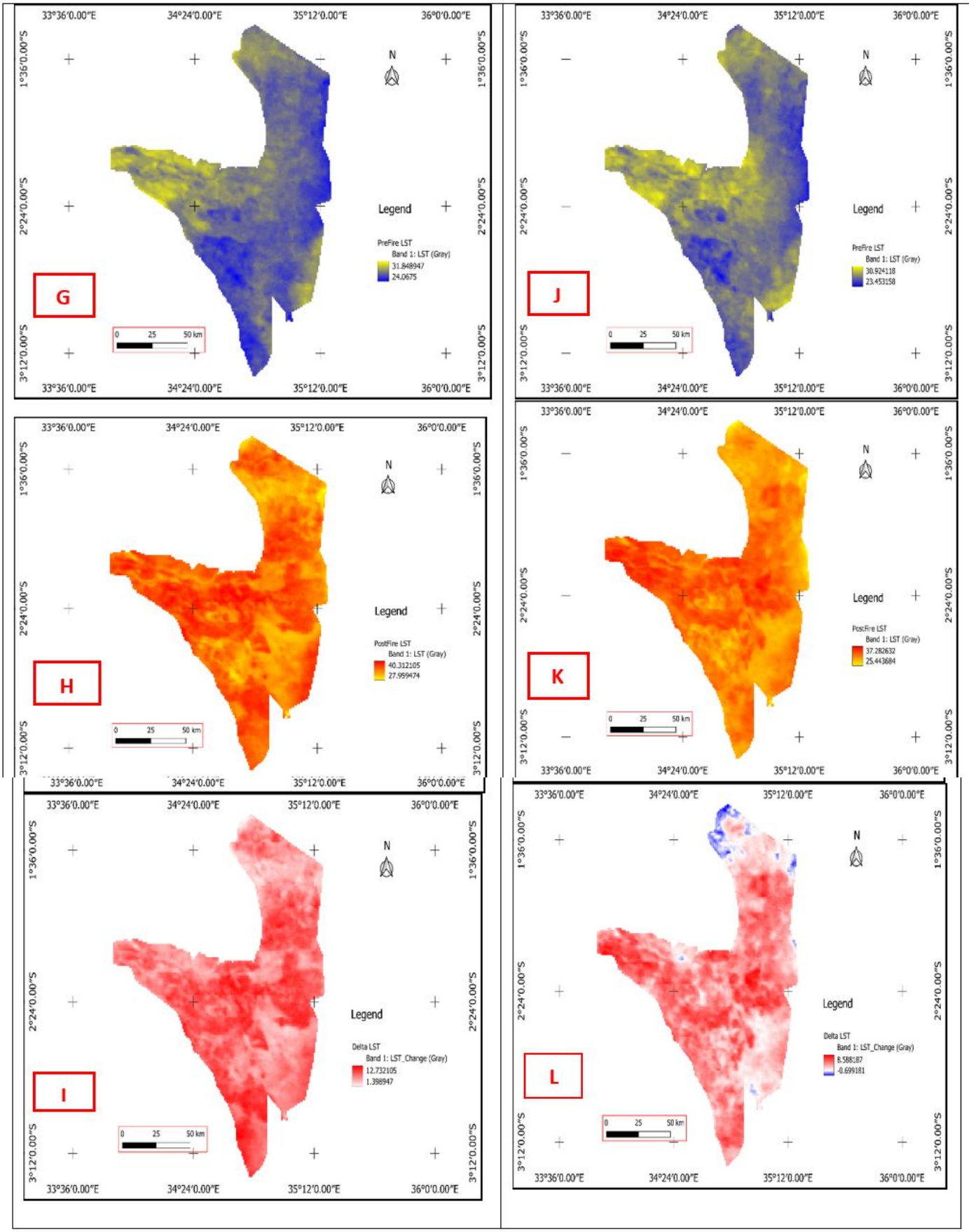

Figure 11. (A) Pre-fire and (B); post-fire LST images of 2001; (C) Delta LST image of 2001; (D) Pre-fire and (E) post-fire LST images in 2010; (F) Delta LST image of 2010; (G) Pre-fire and (H); post-fire LST images of 2020; (I) Delta LST image of 2020; (J) Pre-fire and (K) post-fire LST images in 2024; (L) Delta LST image of 2024

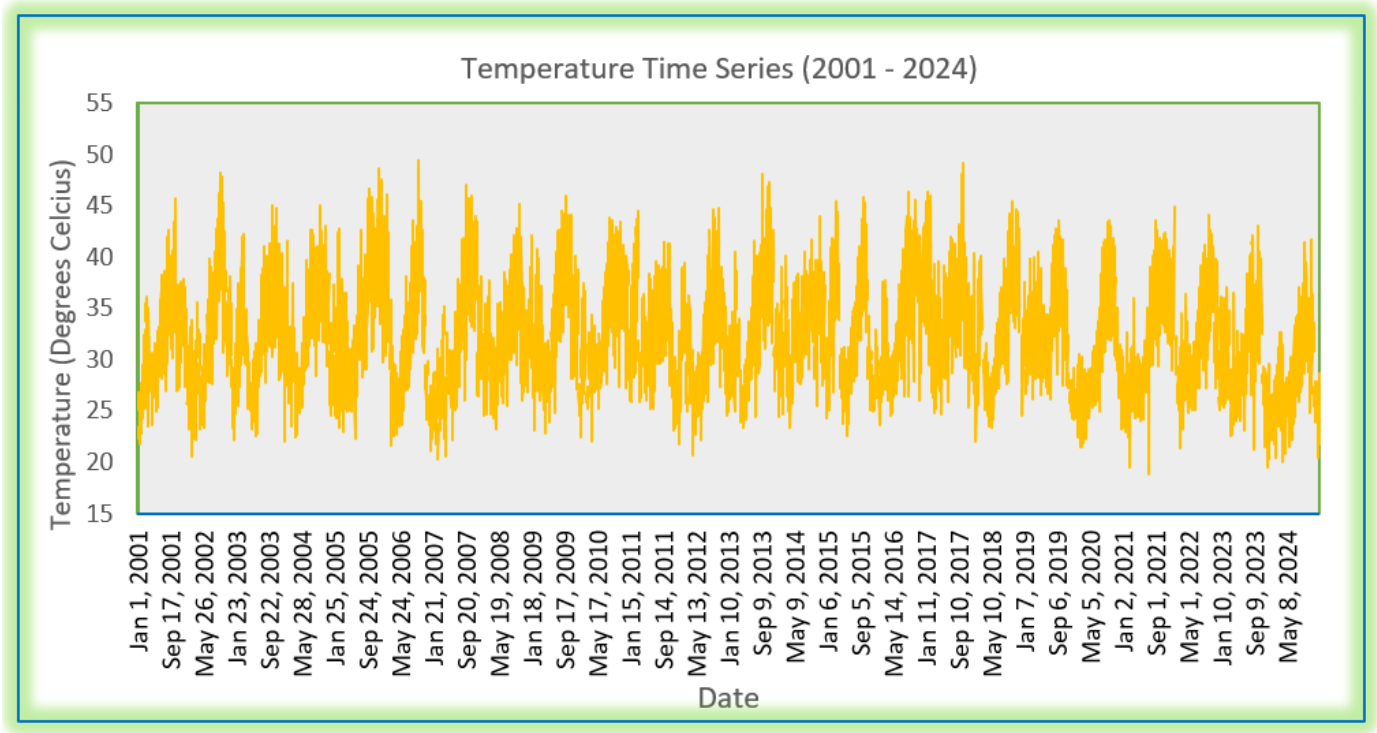

Figure 12. Mean monthly temperature time series from 2001 to 2024

The 2020 pre-fire period was generally cooler across the park, except for low temperatures in the west and some northern and southern areas. Like 2024, the 2020 post-fire period was dominated by low to medium temperatures but was warmer overall than 2024. The 2010 pre-fire period was unique, showing uniformly low temperatures throughout the park. Despite a wide temperature range, most areas remained cool, with some regions experiencing high and medium temperatures. The 2010 post-fire period was the hottest compared to the 2020 and 2024 periods. In 2001, the pre-fire period featured a mix of low, medium, and high temperatures, making it the hottest year overall. Generally, 2024 was the coolest year, while 2001 was the hottest.

The results of the Delta Land Surface Temperature (dLST) in 2024 showed an increase in temperature of 8.588°C, while a decrease of -0.699°C (Fig. 11) was recorded in some parts of the national park. In 2020, the increase in temperature was higher than that of 2024, recorded at 12.732°C, with only a small temperature change (1.398°C) (Fig. 11), indicating a minimal or no change between the pre-fire and post-fire periods. The 2010 dLST also showed a warming trend after the post-fire period, with an increase of 11.698°C, while cold areas recorded a temperature of -0.214°C. In 2001, there was stronger warming and cooling than in other years, with temperatures recorded at 13.86°C for warming and -0.56°C for cooling (Fig. 11). The temperature time series from 2001 to 2024, Fig. 12, depicts the temporal variations in land surface temperature within the study area.

The coolest year within the study period was 2024, and the hottest was 2001 (Fig. 12). A general decline in the maximum Land Surface Temperature (LST) occurred from 2001 to 2024 in both the pre-fire and post-fire periods, although this trend was uneven. Pre-fire LST showed irregular, spatially variable fluctuations. Areas with cooling, mainly in the western, some central, and northern parts of the park, had stable or recovering vegetation. Conversely, regions with significant temperature increases, especially in the southwestern, southern, and eastern zones, showed declines in vegetation cover, indicating a deteriorating vegetation health.

A similar pattern was observed in 2010, especially in the northern and eastern parts, which remained cooler with stable or minimal vegetation changes. In 2020 and 2024, strong cooling and vegetation regrowth were evident in northern areas, reinforcing the close linear relationship between temperature and vegetation density. Dense vegetation absorbs more heat than sparse or bare land. The Serengeti receives much of its water from rivers originating in the north and flowing west to Lake Victoria, which supports a higher vegetation density. Additionally, the western park area remains wet for most parts of the year due to the influence of Lake Victoria, where evaporation boosts local moisture, helping to maintain lower temperatures.

In most cases, the LST-NDVI spatial patterns followed the expected trends, with negative correlations indicating that higher temperatures suppressed vegetation activity (Rahimi et al., 2025). However, this relationship is shaped by factors such as land use change, irrigation, and elevation, which must be considered for accurate interpretation. Urbanization, deforestation, and agricultural expansion alter surface temperatures and vegetation cover, significantly influencing the NDVI-LST relationship (Joshi et al., 2024; Jaafar et al., 2020). In tropical zones, deforestation exposes bare soil, raises LST, and intensifies negative correlations (Li et al., 2016). Around Serengeti National Park, such disturbances, especially farming, grazing, and tree cutting, are common. Stunted tree growth, particularly along the park's eastern and southern edges, reflects these anthropogenic pressures and their role in rising LST.

Prescribed burning in the Serengeti may also contribute to increased surface temperatures. Additionally, heavy grazing by ungulates and habitat disturbances from African elephants reduce vegetation cover, exposing soil and increasing LST. With over 2.5 million large mammals, including grazers, browsers, and carnivores, herbivory significantly shapes vegetation dynamics and biomass loss (IUCN and UNEP-WCMC, 2017). Cooler conditions were generally observed during pre-fire periods, while warmer anomalies occurred in 2001, 2010, and to a lesser extent 2020, often coinciding with low NDVI, especially in the park's southern region.

Anthropogenic disturbances, especially deforestation, drive surface warming in tropical areas with limited seasonality by increasing radiative fluxes (Muro *et al*., 2018; Duveiller et al., 2018; Findell et al., 2017). Vegetation and moisture loss increase LST, whereas the regrowth has a cooling effect (Muro et al., 2018). Deforestation also reduces carbon stocks through increased heterotrophic respiration (Harper et al., 2018). During the dry season (May–October), reduced evapotranspiration post-fire is a key factor in LST increase. The rising temperatures exacerbate evaporation, lower soil moisture, and heighten the risk of droughts and heatwaves (Sharma et al., 2023). These findings underscore how fire and human-driven deforestation contribute to climate feedbacks through interconnected processes (Liu et al., 2018).

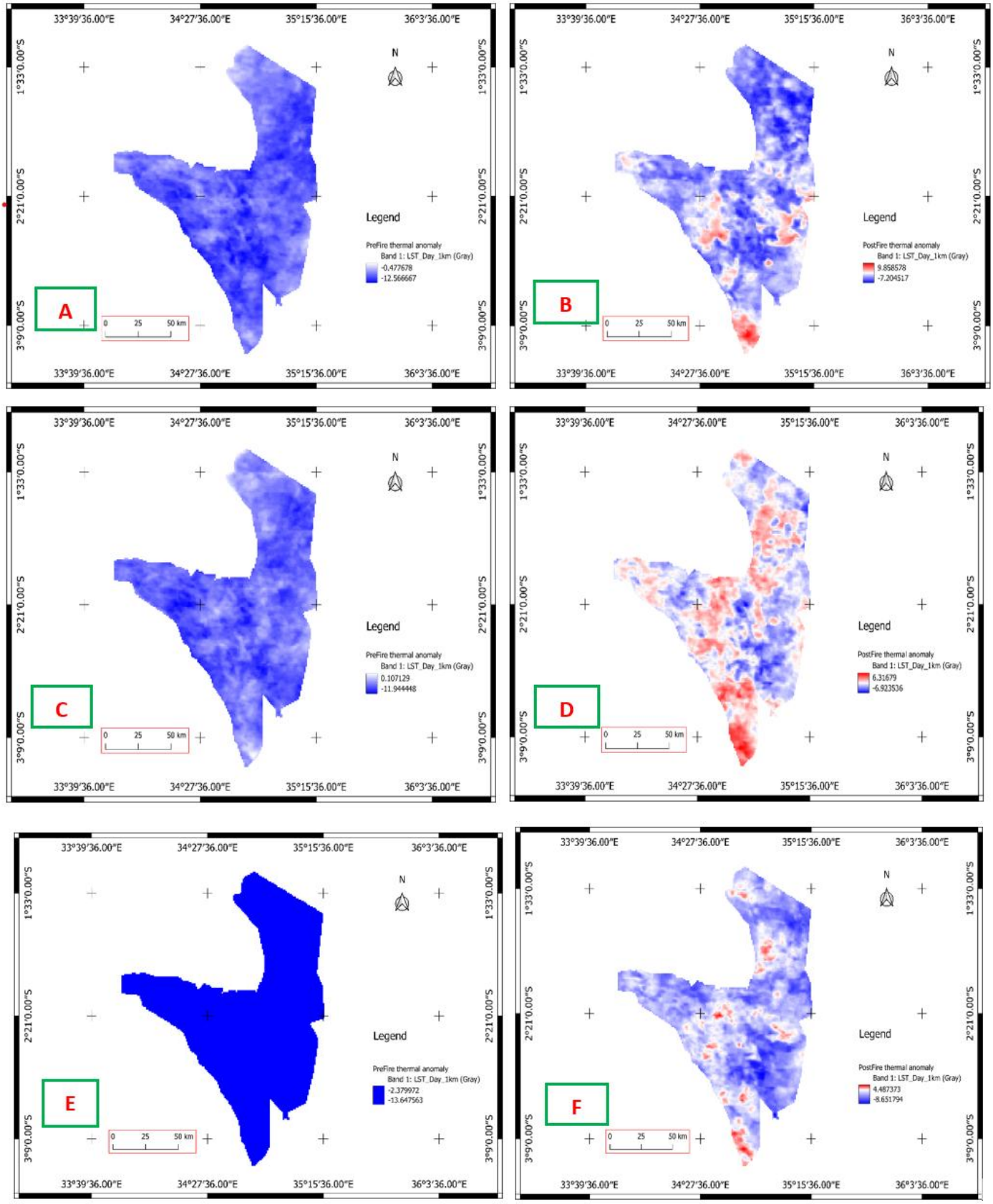
33°39'36.00"E
34°27'36.00"E
35°15'36.00"E
36°3'36.00"E
1°33'0.00"S
2°21'0.00"S
3°9'0.00"S
N
Legend
PreFire thermal anomaly
Band 1: LST_Day_1km (Gray)
-0.477678
-12.566667
A
0 25 50 km
PostFire thermal anomaly
Band 1: LST_Day_1km (Gray)
9.858578
-7.204517
B
0.107129
-11.944448
C
6.31679
-6.923536
D
-2.379972
-13.647563
E
4.487373
-8.651794
F

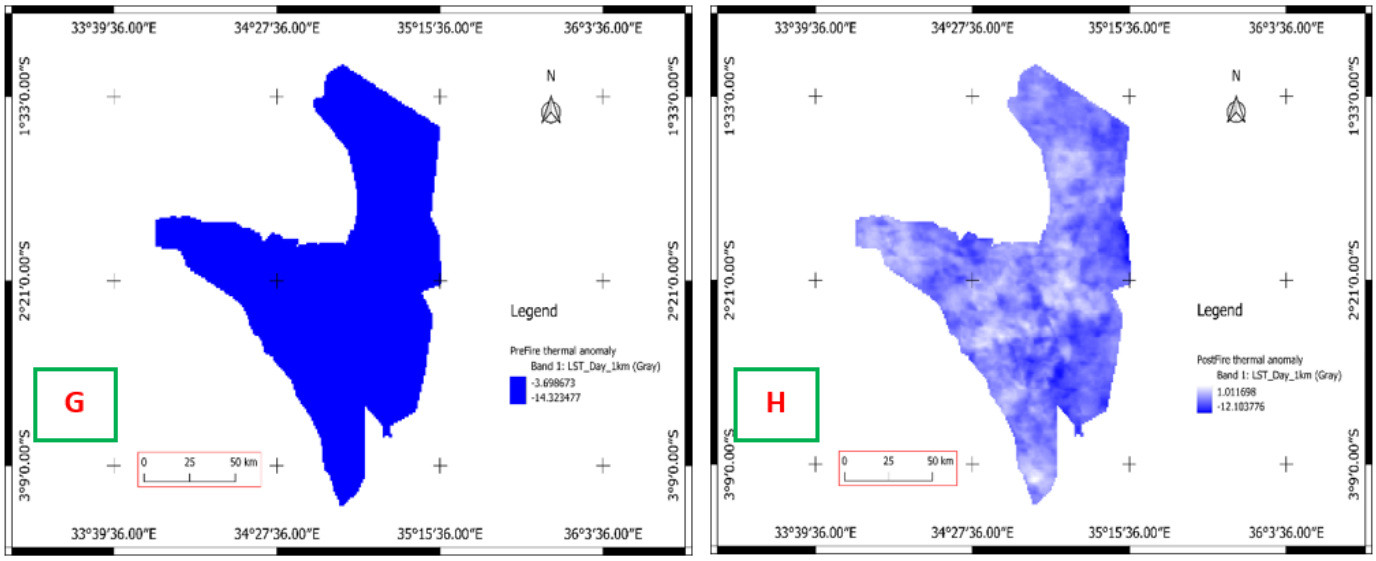

Figure 13. (A) Post-fire Thermal Anomaly 2001; (B) Post-fire Thermal Anomaly 2001; (C) Pre-fire Thermal Anomaly 2010; (D) Post-fire Thermal Anomaly 2010; (E) Pre-fire Thermal Anomaly 2020; (F) Post-fire Thermal Anomaly 2020; (G) Pre-fire Thermal Anomaly 2024; (H) Post-fire Thermal Anomaly 2024.

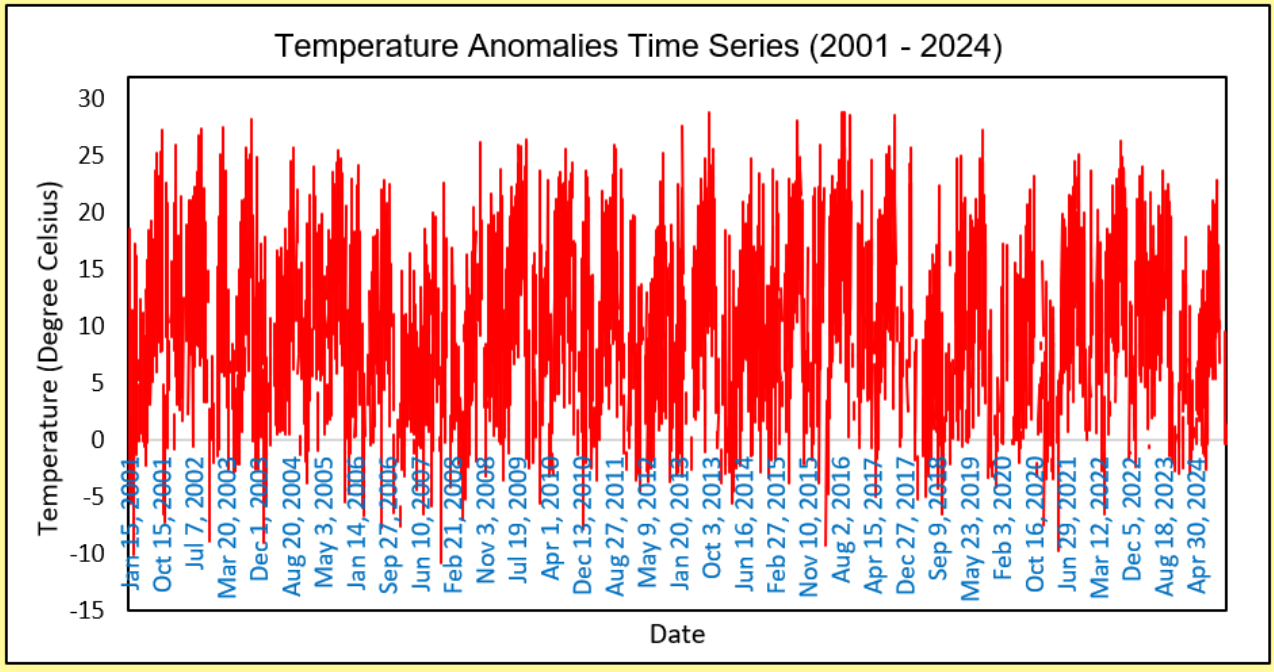

Figure 14. Mean monthly thermal anomaly time series from 2001 to 2024

Relationship Between Burn Severity (dNBR) and Land Surface Temperature (LST)

Based on the dNBR classification by Key and Benson (2006), the burned area was categorized into five severity levels: unburned or regrowth (<100), low (100–270), moderate-low (270–440), moderate-high (440–660), and high severity (≥660). The results indicated that most of the area experienced low to moderate burn severity, with limited zones showing high severity, suggesting that vegetation damage was uneven and recovery potential remained high across much of the landscape. Comparison of LST and dNBR results revealed that areas with higher burn severity (moderate to high dNBR values) corresponded to elevated LST, particularly in the western and central parts of the park.

Conversely, regions with low dNBR values, indicating minimal or no burning, exhibited relatively lower LST. This inverse relationship suggests that fire-induced vegetation loss contributed to increased surface heating, while areas with regrowth or low burn severity showed cooler surface temperatures. Supporting this finding, van der Walt et al. (2018) reported a clear relationship between fire severity and variations in land surface temperature (LST), particularly following the fire season. Areas with higher burn severity showed significant elevated LST, while regions with lower burn severity had comparatively lower LST. These patterns are attributed to the reduced surface emissivity in burned areas and the disruption of the energy balance caused by vegetation loss. A gradual decline in LST was observed in the months after the fire, continuing for up to six months as vegetation regenerated.

Comparative Analysis of Thermal Anomalies (ΔLST) and NDVI

In all years, pre-fire thermal anomalies (Fig. 13) showed cooling or stable temperatures, with 2020 and 2024 dominated by cooling trends, ranging from

–13.65°C to –14.32°C, respectively. The warmest years were 2001 and 2010, where temperatures sharply declined but remained positively above normal, ranging from 9.86°C to 6.32°C. Although 2001 was the warmest year, only a few areas in the east, south, and southwest were extremely hot compared to 2010. In contrast, 2010 had many areas, except parts of the east, north, and west, experiencing much colder conditions. Post-fire anomalies indicated a general warming trend, except for 2024, which was relatively cold, with anomalies ranging from –12.10°C to 1.01°C.

The thermal anomaly time series from 2001 to 2024 was analyzed following the workflow shown in Fig. 14. Thermal anomalies (ΔLST) across the study area, red indicating increased surface temperatures and blue indicating cooling or minimal change, closely align with NDVI patterns. Greenish-yellow tones in the NDVI map (Fig. 15) show healthy vegetation, while reddish-yellow tones indicate reduced cover. Visually, areas with high thermal anomalies (red) generally correspond to lower NDVI values (orange), suggesting vegetation loss drives surface warming. Conversely, cooler anomalies (blue) were associated with higher NDVI values, indicating vegetation preservation or recovery.

Vegetation health and vegetation recovery

Pre-fire NDVI values in 2024 ranged from sparse vegetation (0.059) to dense, healthy vegetation (0.812) (Fig. 15), with moderate levels in between. The post-fire period showed a similar range, from sparse vegetation (-0.741) to dense vegetation (0.729). In 2020, pre-fire NDVI ranged from 0.048 to 0.809, and post-fire values ranged from -0.036 to 0.761. For 2010, pre-fire NDVI ranged from -0.023 to 0.817, while post-fire values ranged from 0.033 to 0.642, indicating sparse to moderate vegetation. In 2001, pre-fire NDVI ranged from -0.006 to 0.802, and post-fire values ranged from 0.046 to 0.656. Overall, 2010 had the highest pre-fire vegetation quality, followed by 2024, though differences across years were small.

High values indicating poor vegetation were recorded in parts of the park in 2010 and 2001. Post-fire, dense, healthy vegetation was more prominent in 2020, while 2024 showed the lowest vegetation quality. The eastern and southern Serengeti were less vegetated during pre-fire periods in 2001, 2010, and 2020 (Fig. 15). The 2024 dNDVI showed little recovery, with some areas in the southwest, east, and north showing minimal change (~0.0377). Much of the park remained stable or showed minor changes, though some areas experienced vegetation loss (dNDVI = -0.452). In contrast, 2020 had small patches of recovery (0.085) (Fig. 15). Overall, large areas remained unchanged or had minimal NDVI variation, with some regions showing decline after fire (dNDVI = -0.479) (Fig. 15). Vegetation recovery in 2010 was similar to 2020. In 2001, a small portion showed vegetation gain (0.058), with other areas showing decline (-0.485) (Fig. 15).

Vegetation recovery, Fig. 16, in SENAPA between 2002 and 2024 exhibited considerable inter-annual variability. Several years, including 2003, 2014, 2018, and 2022, showed negligible recovery, while the most pronounced peaks occurred in 2011 and 2015, with 3,906.5 ha and 6,427.9 ha of recovered vegetation, respectively, indicating substantial post-disturbance regrowth. Most other years recorded moderate recovery, generally below 1,000 ha, highlighting fluctuating ecosystem responses over the 23 years as captured by MODIS NDVI data.

Linking Temperature Contours and Vegetation Density

Fig. 17 clearly shows the relationship between isotherms (temperature contours) and NDVI changes across all years. In 2024, temperature contours aligned with areas of neutral NDVI, whereas in 2020, 2010, and 2001, they overlapped mostly with regions of decreased NDVI, indicating a likely inverse relationship between Land Surface Temperature (LST) and NDVI. Areas with minimal surface temperature changes, such as the northern regions, showed signs of vegetation regrowth. These patterns suggest that rising temperatures correspond with declining NDVI, and vice versa.

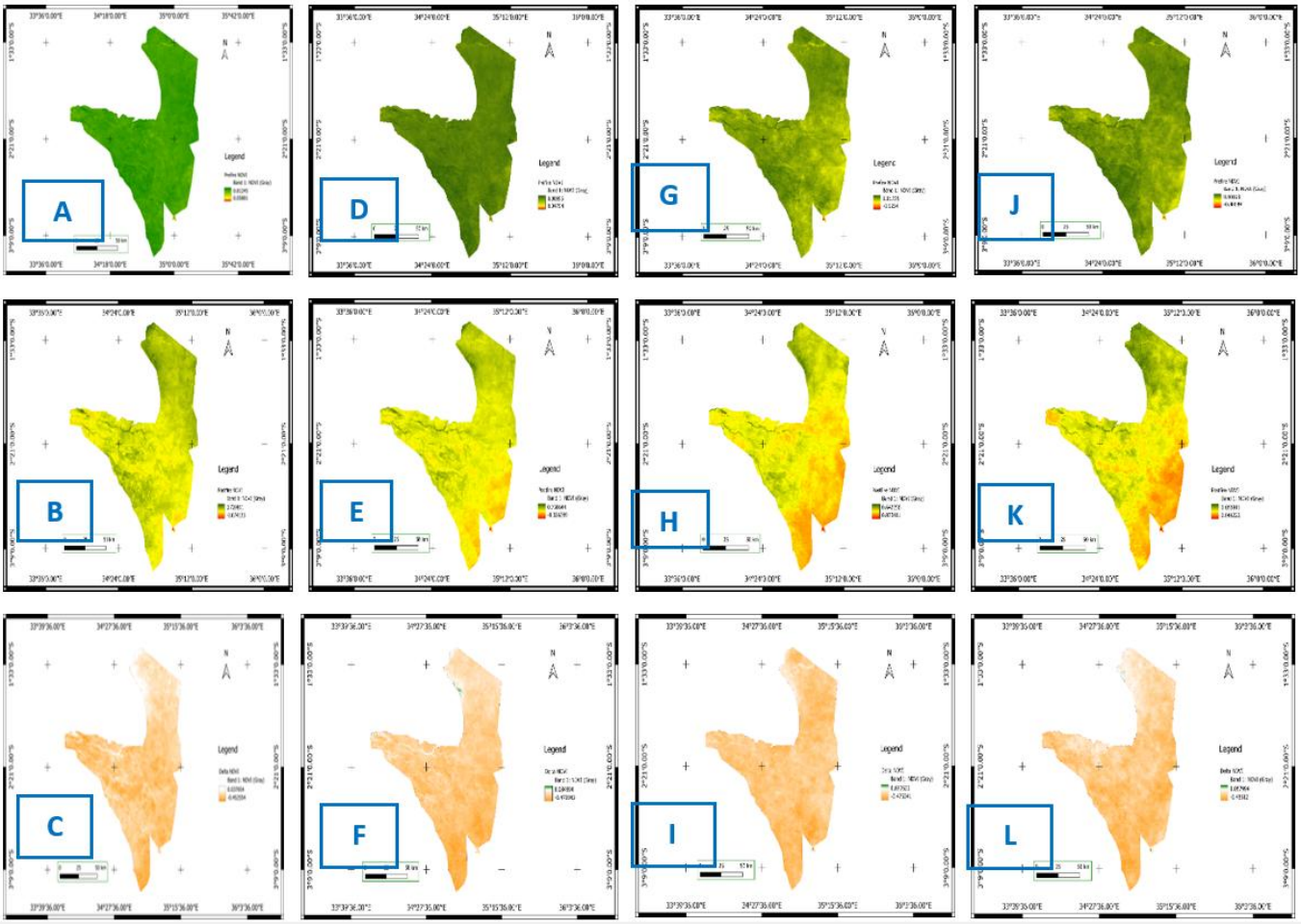

Figure 15. (A) Pre-fire NDVI 2024; (B) Post-fire NDVI 2024; (C) Delta NDVI 2024; (D) Pre-fire NDVI 2020; (E) Post-fire NDVI 2020; (F) Delta NDVI 2020; (G) Pre-fire NDVI 2010; (H) Post-fire NDVI 2010; (I) Delta NDVI 2010; (J) Pre-fire NDVI 2001; (K) Post-fire NDVI 2001; (L) Delta NDVI 2001.

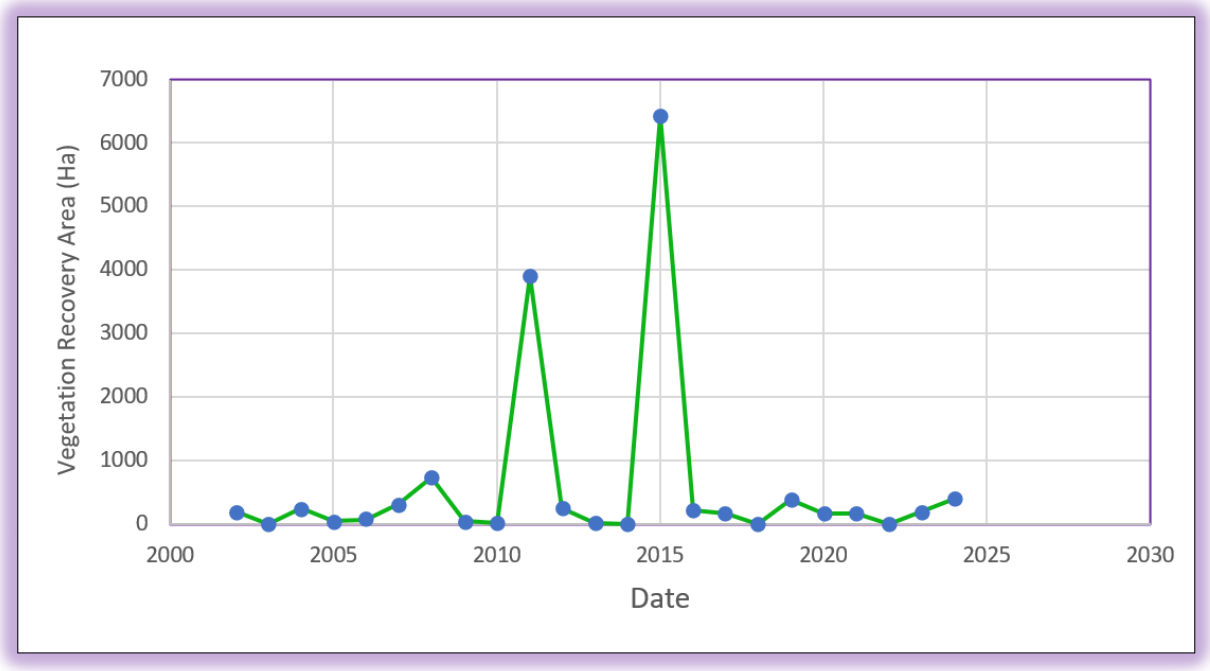

Figure 16. Annual vegetation recovery area (Ha) in SENAPA from 2002 to 2024 based on MODIS NDVI

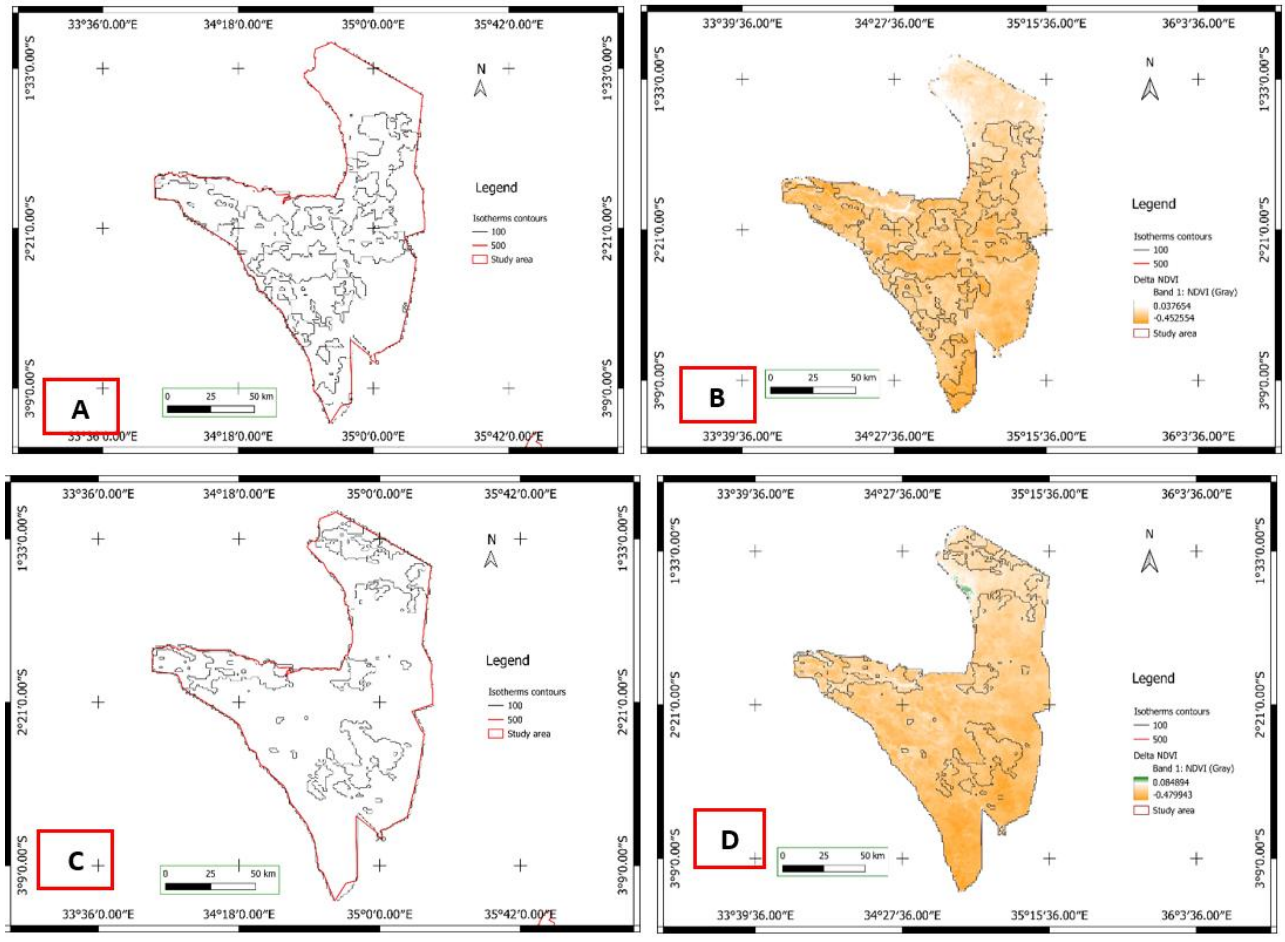

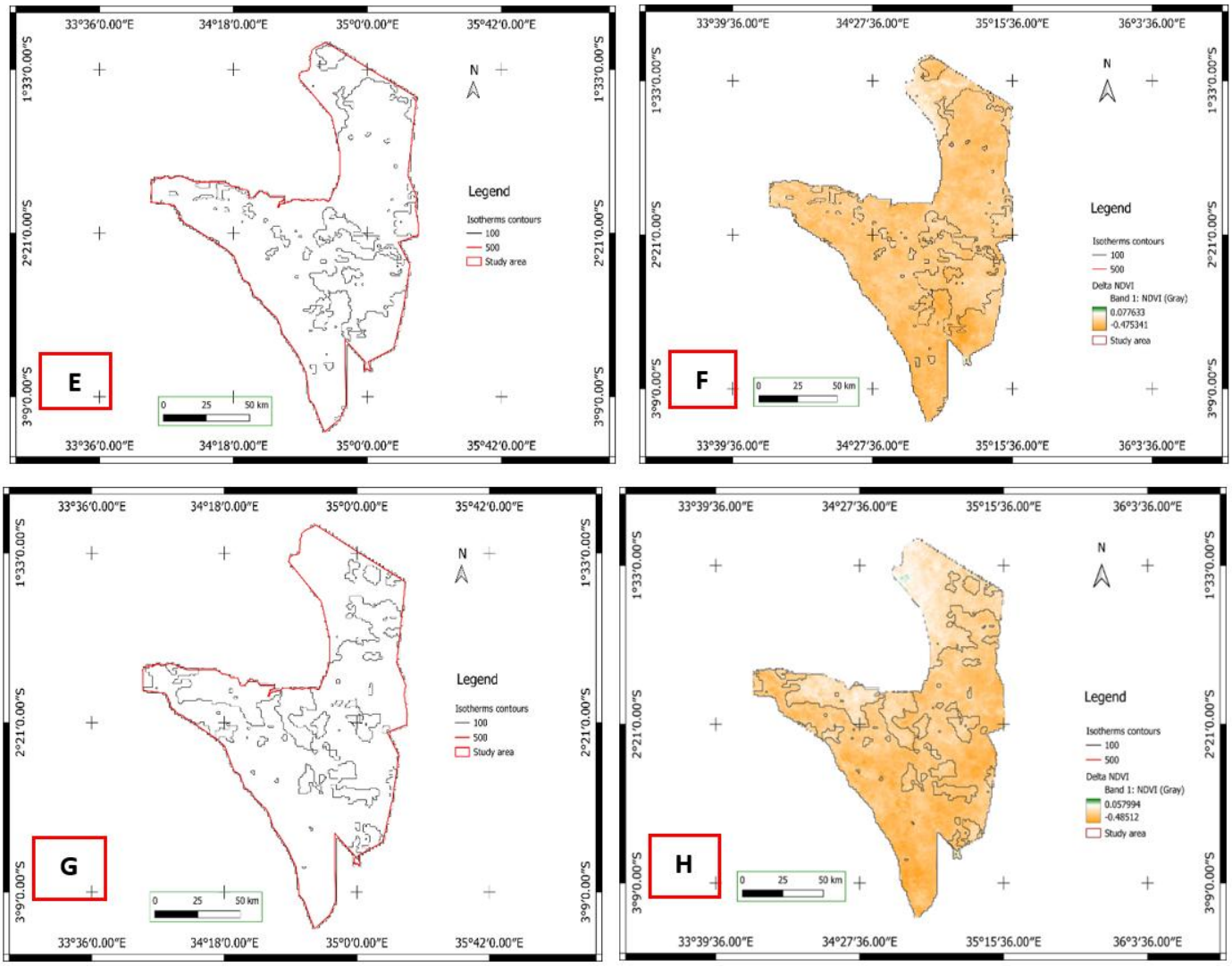

Figure 17. (A) Temperature Contour (Isotherm) Map 2024; (B) ΔNDVI–LST Contour Composite Map 2024; (C) Temperature Contour Map 2020; (D) ΔNDVI–LST Contour Composite Map 2020; (E) Temperature Contour Map 2010 (F) ΔNDVI–LST Contour Composite Map 2010; (G) Temperature Contour Map 2001 (H) ΔNDVI–LST Contour Composite Map 20001.

The spatial relationship between post-fire thermal anomalies and NDVI, notably in 2010, underscores the ecological impact of the fires. Vegetation loss diminishes canopy cover and evapotranspiration, contributing to increased Land Surface Temperature (LST), which consequently aligns low NDVI with high thermal anomalies. Conversely, cooler areas overlapping with higher NDVI values likely represent regions unaffected by fire or where vegetation recovery has begun, helping to regulate surface temperatures. The discrepancies between thermal anomalies and NDVI may result from factors such as soil moisture variation, topography, or differing recovery rates among vegetation types. Additionally, residual heat from burned biomass and changes in post-fire land cover, such as increased bare soil, can independently affect LST, accounting for the mismatches in thermal and NDVI patterns.

Changes in vegetation cover alter the surface's radiative and non-radiative properties, influencing the Earth's energy balance through region- and season-specific biophysical processes that can lead to warming or cooling, depending on vegetation type and climate as articulated in (Duveiller et al., 2018). Forested areas and water bodies consistently showed lower Land Surface Temperature (LST) during both pre- and post-fire periods. Strong negative correlations between LST and NDVI were observed post-fire, while pre-fire periods showed moderate inverse correlations, probably due to the enhanced vegetation from rainfall. Overall, LST and NDVI maintained a consistent inverse relationship (Kikon et al., 2023).

Before prescribed fires, a written and approved burn plan must define acceptable weather and fuel conditions, desired fire behavior, and ecological goals (Kupfer et al., 2020). These parameters, known as the prescription burn window, include weather, fuel moisture, and other key factors, and must be strictly followed to ensure safety and effectiveness (Schweizer and Cisneros, 2017; Budd, 2001). In Serengeti National Park, LST and NDVI analyses highlight the importance of aligning prescribed burns with ecologically appropriate conditions. To ensure responsible fire management, authorities should set clear baselines, improve data systems, and enforce best practices.

The eastern and southern regions of the park should be prioritized for early prescribed burns, as delayed burning may harm fire-sensitive species. These areas show post-fire vegetation stress, likely due to sparse cover, low rainfall, rocky terrain, and deforestation. Burning before the dry season can help preserve forage and ecosystem services until the short rains. After these zones, the central region should be treated. In contrast, the northern, western, and southwestern areas, characterized by high NDVI, better vegetation health, and likely higher rainfall, should be burned later in the season when the conditions are the driest in order to maximize fuel efficiency and ecological outcomes. Based on the precipitation results, lower precipitation during dry seasons likely increases fire risk, whereas higher rainfall periods likely enhance post-fire vegetation regrowth. Variability in rainfall affects the timing and effectiveness of prescribed burns and the resilience of recovering vegetation.

Precipitation and Soil Moisture as a Determinants of Land Surface Temperature Patterns

Monthly mean precipitation from 2001 to 2024 (Fig. 18) exhibited strong seasonal fluctuations and interannual variability, with the wet-season peaks and dry-season troughs, but no clear long-term trend. These rainfall patterns influence the health of vegetation, soil moisture, and consequently Land Surface Temperature (LST). Observed LST values showed that pre-fire temperatures ranged from 23.45–35.69°C and post-fire temperatures range from 25.44–42.76°C, with higher post-fire LST generally occurring in drier periods or regions with lower vegetation cover. Cooler pre-fire temperatures typically coincided with wetter months and areas with higher soil moisture, while elevated LST during dry periods reflected reduced evaporative cooling. Linking precipitation, vegetation, and soil moisture thus, helps explain the spatial and temporal variability in LST, providing a basis for predictive modeling.

Figure 19 illustrates the temporal variation of mean soil moisture (SM) at three depths (0–10 cm, 10–40 cm, and 40–100 cm) from 2001 to 2024. Overall, soil moisture showed clear seasonal and interannual fluctuations across all layers. The shallow layer (0–10 cm) exhibited the greatest variability, with pronounced peaks and declines corresponding to wet and dry periods. The intermediate layer (10–40 cm) maintained moderate moisture levels with smoother fluctuations, while the deepest layer (40–100 cm) displayed more stable patterns and lower moisture content, particularly during extended dry periods. Notable increases in soil moisture occurred around 2006–2007, 2017–2018, and 2020–2021, aligning with wetter climatic conditions, whereas significant decreases were observed during prolonged dry intervals, such as 2004–2005 and 2012–2013.

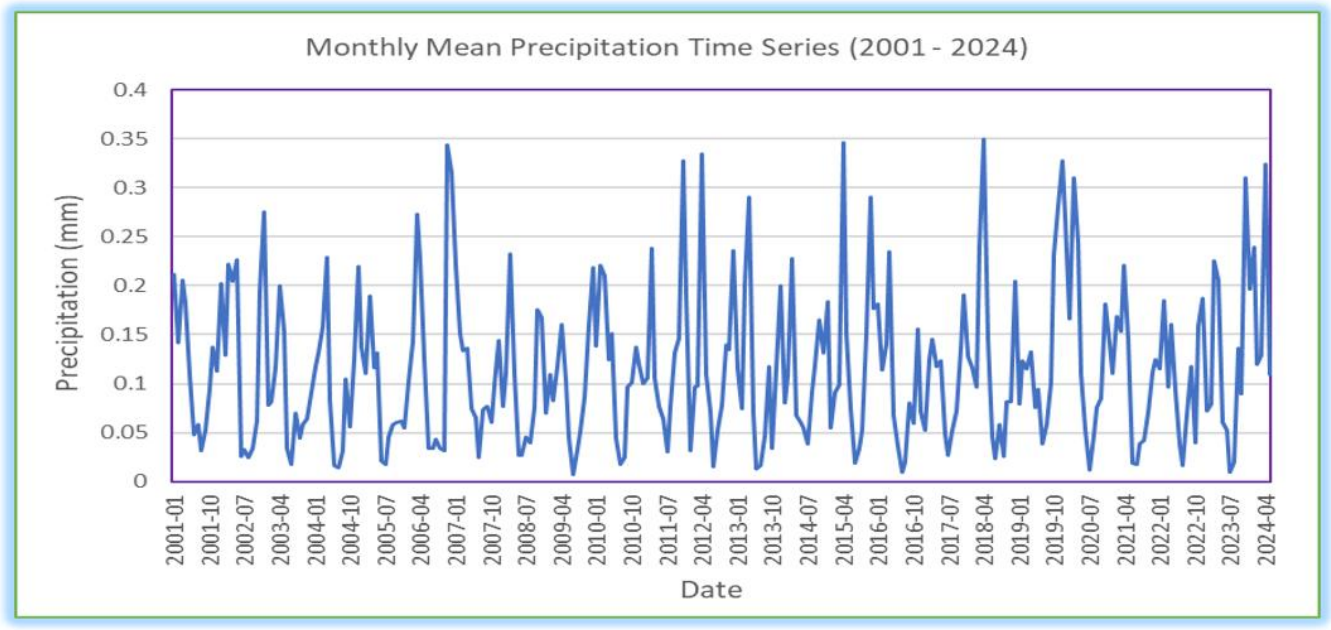

Figure 18. Monthly mean precipitation from 2001 to 2024

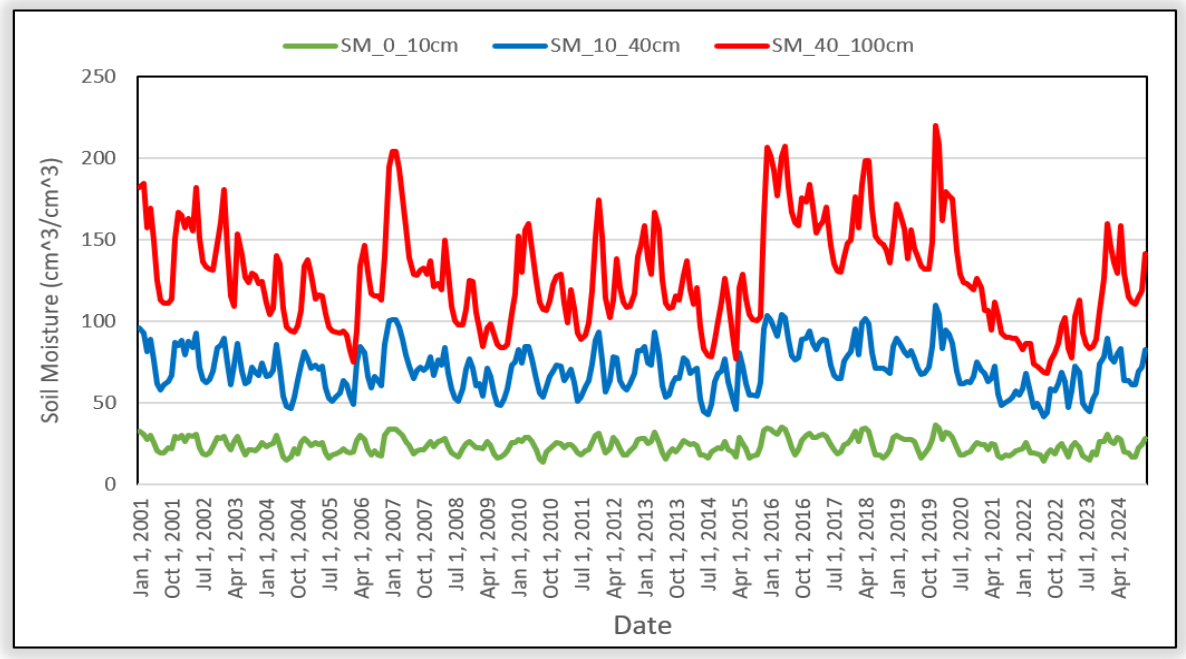

Figure 19. Temporal variation of mean monthly soil moisture at three depths (0–10 cm, 10–40 cm, and 40–100 cm) from 2001 to 2024 within the study area.

The temporal patterns indicate that soil moisture dynamics are primarily governed by rainfall variability and soil depth. The surface layer responds rapidly to the precipitation and evaporation, exhibiting pronounced short-term fluctuations, whereas deeper layers retain moisture longer and act as buffers against transient climatic variations. Shallow soils are more sensitive to atmospheric forcing (e.g., temperature, radiation, and evapotranspiration), while deeper layers reflect longer-term hydrological processes. Soil structure plays a key role in determining how precipitation is divided between infiltration and runoff. Moisture retained in the root zone is available for plant uptake and can be transpired back to the atmosphere, while water that moves past the root zone travels through the vadose zone into the saturated zone, recharging groundwater (Reinsch et al., 2024).

An inverse relationship between soil moisture (SM) and land surface temperature (LST) was observed, which was consistent with the surface energy balance principles. During dry periods, limited soil moisture reduces evaporative cooling, resulting in elevated LST, whereas higher moisture enhances latent heat flux and moderates surface warming. SM will lead to an increase in land surface sensible heat flux and, thus, a rise in LST, with the increased LST further accelerates land surface evaporation, leading to lower SM (Jiang et al., 2023). More water enters the atmosphere in a warming world leading to an increase in radiative feedback (Jiang et al., 2023). This interaction was particularly evident in years such as 2004–2005, 2012–2013, and 2018–2019, when low soil moisture coincided with positive temperature anomalies. The upper soil layer (0–10 cm) demonstrated the strongest and most immediate response to temperature changes, emphasizing its close coupling with atmospheric conditions.

In contrast, deeper layers acted as moisture reservoirs, delaying depletion and dampening thermal variability. This depth-dependent response corroborates earlier studies that asserted that near-surface soil moisture governs short-term thermal behavior, whereas deeper layers influence long-term land–atmosphere feedbacks. The increased frequency of temperature anomalies after 2015 may indicate an intensified warming and declining soil water retention, potentially linked to the shifts in rainfall regimes, vegetation cover, or land-use practices. These findings underscore the need to incorporate soil moisture variability into LST prediction models, as neglecting these interactions can lead to significant biases in estimating surface temperature dynamics.

Contribution of Vegetation Variability to Land Surface Temperature Modeling

The total area of the study site was approximately 1,312,179.12 ha (13,121.79 square kilometers). Across the study period from 2002 to 2024, Grasslands overwhelmingly dominated the study area between 2002 and 2020, Table 2a and 2b, consistently covering around 99% of the total area, with a slight decline to 99.2% by 2020. Savannas gradually expanded from 0.1% in 2002 to 0.6% in 2020. Cropland area showed notable fluctuations, including a sharp drop from 15,221 ha (1.17%) in 2002 to 2,123–2,676 ha (0.16–0.21%) in 2006, followed by minor increases in subsequent years. Permanent wetlands and barren areas remained minimal (<0.03%), and unclassified areas disappeared after 2006.

The landscape remained largely dominated by grasslands, with gradual encroachment of savannas and intermittent changes in cropland extent. The sudden reduction of croplands and disappearance of unclassified areas in 2006 may reflect land-use reclassification, natural vegetation succession, or improved mapping accuracy. Overall, the land cover remained stable over two decades, with localized transitions likely influenced by human activities, fire regimes, or ecological succession. A study by Gizachew et al. (2020), in Tanzania, revealed that Game Controlled Areas (GCAs) presented the highest area-weighted mean annual deforestation, followed by Forest Reserves (FRs), Game Reserves (GRs), and National Parks (NPs); while Forest Plantations and Nature Reserves exhibit the lowest. In East Africa, the Serengeti ecosystem in Northern Tanzania is experiencing significant land-use changes, particularly due to increased anthropogenic pressures along its borders, mainly agriculture and settlements, and changes in various national policies (Veldhuis et al., 2019). Understanding the spatial and temporal dynamics of habitat quality is fundamental to effective management of the ecosystems experiencing changing land use and cover (Kija et al., 2020).

Table 2a. Temporal changes in land cover area (ha) and percentage of total within the study area (2002–2020)

Year	Grasslands		Savannas		Croplands	
	Area (ha)	% of Total	Area (ha)	% of Total	Area (ha)	% of Total
2002	1289301.212	98.698	1388.959	0.106	15221.120	1.165
2004	1302689.559	99.724	521.165	0.039	2675.768	0.205
2006	1303276.397	99.768	511.820	0.039	2123.074	0.162
2008	1304328.426	99.849	754.986	0.058	827.879	0.063
2010	1304435.341	99.857	928.661	0.071	547.290	0.042
2012	1303790.339	99.808	1151.915	0.088	969.037	0.074
2014	1303090.722	99.754	1077.439	0.082	1743.130	0.133
2016	1301245.215	99.613	1052.695	0.080	3613.381	0.277
2018	1303178.000	99.761	1226.635	0.094	1531.456	0.117
2020	1295884.317	99.203	7991.423	0.612	2085.151	0.159

Table 2b. Temporal changes in land cover area (ha) and percentage of total within the study area (2002–2020)

Year	Permanent Wetlands		Barren		Unclassified	
	Area (ha)	% of Total	Area (ha)	% of Total	Area (ha)	% of Total
2002	24.799	0.002	339.217	0.026	24.799	0.002
2004	24.799	0.002	364.017	0.028	24.799	0.002
2006	49.599	0.004	339.217	0.026	-	-
2008	49.599	0.004	339.217	0.026	-	-
2010	49.599	0.004	339.217	0.026	-	-
2012	49.599	0.004	339.217	0.026	-	-
2014	49.598	0.004	339.217	0.026	-	-
2016	49.599	0.004	339.217	0.026	-	-
2018	123.997	0.009	240.019	0.018	-	-
2020	223.195	0.017	116.023	0.009	-	-

Table 3 summarizes the temporal variation in predictor variables and Land Surface Temperature (LST) from 2002 to 2024. Mean burn severity (dNBR) from Sentinel-2 and MODIS (MOD09A1) shows temporal variability. Sentinel-2 data (2018–2024) range from 0.034 to 0.467, while MODIS values range from −0.418 to −0.214, with 2024 MODIS data unavailable. Analysis of biennial data from 2002 to 2024 revealed temporal variation in burn severity, quantified using both MODIS dNBR and Sentinel-2 indices, alongside corresponding LST statistics. MODIS-derived mean dNBR indicates predominantly low to moderate-low severity burns (Key & Benson, 2006), whereas Sentinel-2 shows positive indices (0.146–0.457) in later years, reflecting post-fire vegetation changes. Observed LST remained relatively stable (29.2–34.5 °C), though years with higher burn severity, such as 2020 (dNBR = −0.418), corresponded to slightly lower temperatures, likely due to reduced vegetation cover. Overall, burn severity influenced surface thermal conditions, modulated by vegetation recovery, soil moisture, and land cover heterogeneity.

Sentinel-2 was used independently for the dNBR assessment. Although it was not included in the LST model validation due to its lack of coverage in the early 2000s, thereby avoiding an incomplete accuracy estimate, it was still utilized as a finer-resolution dataset to support the multi-year fire trend analysis, which incorporated MODIS datasets among others. The negative MODIS dNBR values, in contrast to the positive values from Sentinel-2, are primarily due to differences in spatial resolution, spectral bands, and temporal compositing. MODIS' coarser 1 km resolution and broader NIR/SWIR bands average over heterogeneous landscapes, sometimes capturing early vegetation recovery in the post-fire period, which can result in slightly negative dNBR. Sentinel-2, with finer spatial resolution (10–20 m) and narrower bands, detects sharper local burn contrasts, producing positive dNBR values shortly after fire events.

Elevated LST years (e.g., 2006, 2016) coincided with lower NDVI recovery, indicating vegetation stress, while cooler years (2020, 2024) corresponded to higher NDVI recovery, reflecting partial post-fire regrowth. The mean volumetric soil moisture across the study area varied over the 2002–2024 period, with values in the top 0–10 cm layer ranging from 0.1986 to 0.2862 m^3/m^3, in the 10–40 cm layer from 0.5394 to 0.9080 m^3/m^3, and in the 40–100 cm layer from 0.7844 to 1.8283 m^3/m^3. Soil moisture in the earlier years (2002–2012) was generally lower in deeper layers (10–100 cm), while the topsoil (0–10 cm) remained relatively stable, averaging around 0.23 m^3/m^3. Corresponding mean land surface temperature (LST) values ranged from 29.2 °C to 34.5 °C, with median values closely matching the means. Notably, higher soil moisture in deeper layers (e.g., 0.908 m^3/m^3 in 2016) coincided with the highest observed LST (34.5 °C), while lower deep-soil moisture in 2024 (0.784 m^3/m^3) coincided with the lowest LST (29.2 °C), indicating a potential inverse relationship between deep-soil moisture and surface temperature over time.

The observed patterns suggest that variations in soil moisture, particularly in deeper layers, may influence surface energy balance and modulate land surface temperatures. Higher deep-soil moisture likely enhances soil heat capacity and evaporative cooling, contributing to elevated LST when combined with other environmental factors, whereas lower deep-soil moisture reduces this buffering effect, resulting in lower LST. These findings highlight the importance of considering soil moisture profiles when assessing temporal LST dynamics and fire recovery impacts in semi-arid landscapes. The results indicate a clear inverse relationship between soil moisture and temperature, where increases in soil moisture corresponded with decreases in soil temperature. This negative correlation is largely due to the higher heat capacity of water compared to soil, which allows soil moisture to strongly regulate thermal conditions (Zhang et al., 2020). Reductions in soil moisture can lead to notable local warming effects.

The Shannon Diversity Index (SDI) values for the study area, calculated from 2002 to 2020, ranged from 0.013 to 0.075, indicating generally low to moderate heterogeneity in land cover types. Mean SDI was highest in 2002 (0.075) and 2020 (0.053), while the lowest values were observed between 2008 and 2010 (0.013), suggesting periods of lower landscape diversity. Corresponding mean Land Surface Temperatures (LST) varied between 29.2°C and 34.5°C, with median LST values showing a similar pattern. Periods with slightly higher SDI generally coincided with moderate LST values, suggesting that landscapes with greater land-cover diversity may contribute to local thermal regulation through shading, evapotranspiration, and surface heterogeneity. Conversely, lower SDI values were associated with more extreme LSTs, reflecting the influence of more homogeneous land surfaces on thermal dynamics. Data for 2022 and 2024 were unavailable or could not be reliably computed. Overall, the SDI values exhibited minimal temporal variation, indicating that the landscape has undergone limited structural change during the study period and is dominated by a few land-cover types with low evenness and richness.

Such low compositional diversity likely corresponds to homogeneous vegetation cover or disturbed areas with reduced ecological complexity. These observations align with findings by Xie et al. (2018), who reported a strong negative correlation between mean NDVI and LST across various land-cover types, particularly in relatively homogeneous landscapes such as built-up and dense forest areas, whereas grasslands exhibited weaker correlations, likely due to higher internal heterogeneity and complex vegetation structure. Collectively, these results reinforce the role of vegetation density and spatial uniformity in modulating surface temperature patterns.

Table 3. Temporal variation in predictor variables and Land Surface Temperature (LST) from 2002 to 2024

Year	NDVI Recovery Mean (index)	NDVI Recovery Median (index)	Shannon Diversity Mean (index)	Mean volumetric soil moisture in the top 0–10 cm (m^3/m^3)	Mean volumetric soil moisture in 10–40 cm depth (m^3/m^3)	Mean volumetric soil moisture in 40–100 cm depth (m^3/m^3)	Burn Severity Mean – Sentinel-2 (index)	Burn Severity Mean – MODIS (index)	LST Mean (°C)	ST Median (°C)
2002	-0.292	-0.299	0.075	0.25074	0.76964	1.50169	-	-0.296	33.017	33.031
2004	-0.235	-0.240	0.021	0.21971	0.64247	1.10101	-	-0.214	33.499	33.467
2006	-0.261	-0.259	0.018	0.23133	0.69319	1.19034	-	-0.280	34.034	34.092
2008	-0.200	-0.205	0.013	0.22820	0.66037	1.14725	-	-0.273	32.758	32.906
2010	-0.268	-0.267	0.013	0.22677	0.68985	1.26927	-	-0.348	33.656	33.657
2012	-0.175	-0.181	0.017	0.22574	0.67509	1.20008	-	-0.319	32.462	32.406
2014	-0.174	-0.166	0.020	0.21343	0.61169	1.01885	-	-0.256	33.436	33.593
2016	-0.292	-0.299	0.029	0.28618	0.90804	1.82833	-	-0.237	34.539	34.591
2018	-0.278	-0.283	0.019	0.25019	0.82009	1.62725	0.146	-0.379	33.278	33.283
2020	-0.255	-0.256	0.053	0.24732	0.76650	1.49895	0.457	-0.418	31.252	31.282
2022	-0.254	-0.256	-	0.19861	0.53938	0.78441	0.307	-0.287	32.571	32.594
2024	-0.246	-0.256	-	0.23510	0.72930	1.31578	0.314	-	29.231	29.108

The Shannon Diversity Index (H′) (Table 3), measures ecosystem diversity based on species richness and evenness. Values of $H' \leq 1$ indicate *low diversity*, $1 < H' \leq 3$ indicate *moderate diversity*, and $H' \geq 3$ represent *high diversity*, with higher values reflecting more balanced and diverse communities (Ulfah et al., 2019). The values of Simpson's Diversity Index (D) usually range between 0 and 1. A higher D indicates a more diverse community, with increasing diversity generally suggesting a more stable ecosystem and stronger interconnections within it (Sharashy, 2022).

NDVI recovery values ranged from −0.292 to −0.174 (mean) and −0.299 to −0.166 (median), indicating overall post-fire reductions in vegetation. These results suggest a partial vegetation recovery across the study period, with some areas experiencing persistent stress. Overall, NDVI recovery and soil moisture emerged as primary drivers of LST. Reduced NDVI recovery was associated with higher LST, highlighting the cooling effect of healthy vegetation through shading and evapotranspiration. The stability of soil moisture and land-cover heterogeneity indicates that microclimatic variations were largely driven by vegetation condition rather than landscape composition. These results demonstrate the effectiveness of NDVI recovery and soil moisture as predictors in LST modeling, providing a robust framework for assessing thermal dynamics in post-fire savanna landscapes.

Conclusions and Recommendations

The analysis of Land Surface Temperature (LST), thermal anomalies, and NDVI from 2001, 2010, 2020, and 2024 has revealed the key impacts of fire on Serengeti National Park. The model showed strong predictive accuracy with a high R^2 and low errors. LST exhibited substantial temporal variability, with 2001 emerging as the warmest year and 2024 the coolest. Post-fire warming trends were most pronounced in 2001, whereas 2024 showed cooler anomalies. Thermal anomalies closely aligned with vegetation loss, reaffirming the regulatory role of vegetation in moderating surface temperatures. NDVI patterns indicated healthier vegetation conditions in 2010, followed by a marked decline in 2024, with only limited recovery evident in 2020 and 2024. Both isotherm distributions and NDVI dynamics further supported the inverse relationship between temperature and vegetation cover. The findings underscore that LST in the study area is driven by complex interactions among soil moisture, vegetation, and fire. Shallow soils responded rapidly to precipitation, with low moisture levels contributing to elevated surface temperatures, while deeper soil layers mitigated short-term fluctuations. Higher LST consistently corresponded with reduced NDVI recovery and lower soil moisture, whereas cooler periods coincided with partial vegetation regrowth and greater moisture availability, particularly at depth. Burn severity, derived from Sentinel-2 and MODIS dNBR, also shaped local LST patterns, with high-severity burn areas exhibiting slightly lower surface temperatures due to vegetation loss and increased post-fire soil exposure. The dominance of grasslands, alongside sparse savannas, croplands, wetlands, and barren areas, contributes to higher and more variable LST. Lower SDI values were associated with more extreme LSTs, reflecting the influence of more homogeneous land surfaces on thermal dynamics. Effective fire management, such as timing prescribed burns according to seasonal and regional conditions, combined with monitoring using LST and NDVI, can support vegetation recovery, reduce temperature extremes, and enhance ecosystem resilience.

The recommendations from this study emphasize that fire management in Serengeti National Park should be tailored to seasonal and regional conditions, with prescribed burns conducted shortly after the short rainy season in the eastern, southern, and central regions to reduce vegetation stress and support herbivore forage, while delaying burns in the wetter northern, western, and southwestern areas to optimize fuel conditions and enhance ecosystem resilience. Post-fire restoration efforts should prioritize areas exhibiting limited vegetation recovery, particularly following the 2020 and 2024 fires, through measures such as preventive fire management and erosion control to facilitate natural regeneration. Future studies should incorporate additional predictors, such as topography and surface albedo, to better capture local LST variability and reduce residual errors. Employing a non-linear supervised learning approach, such as Random Forest Regression (RFR), could improve model performance by accounting for complex interactions among predictors and addressing the moderate explanatory power and unexplained local temperature variations observed in the current linear model. Finally, I recommend that active engagement of local communities and stakeholders is essential to align ecological objectives with safety and socioeconomic considerations.

Conflict of Interest

The authors declare no conflict of interest.

References

Agbor, C. F., and Makinde, E. O. (2018). Land Surface Temperature Mapping using geoinformation techniques. *Geoinformatics FCE CTU* 17(1), 12–25.https://doi.org/10.14311/gi.17.1.2.

Anderson, T. M., Ritchie, M. E, Mayemba, E. Eby, S., Grace, J. B., McNaughton, S. J., et al. (2007). Forage nutritive quality in the Serengeti ecosystem: The roles of fire and herbivory. *The American Naturalist,* 170(3),343–357. https://doi.org/10.1086/520120.

Bindajam, A. A., Mallick, J., AlQadhi, S., Singh, C.K. and Hang, H. T. (2020). Impacts of vegetation and topography on Land Surface Temperature variability over the semi-arid Mountain Cities of Saudi Arabia. *Atmosphere*, 11(7), 1-28.https://doi.org/10.3390/atmos11070762.

Bonan, G. B. (2008). Forests and climate change: Forcings, feedbacks, and the climate benefits of forests. *Science*, 320(5882), 1444–1449.https://www.science.org/doi/10.1126/science.1155121.

Bond, W. J., and Keane, R. E. (2017). *Fires, ecological effects of. Reference Module in Life Sciences*, 1–11. https://doi.org/10.1016/B978-0-12-809633-8.02098-7.

Botha, N., H. Job, and Kimario, F. (2021). Potential and challenges of the Serengeti-Ngorongoro Biosphere Reserve, Tanzania. *eco.mont*, 13, special issue. https://dx.doi.org/10.1553/eco.mont-13-sis27.

Budd, G. M. (2001). How do wildland firefighters cope? Physiological and behavioural temperature regulation in men suppressing Australian summer bushfires with hand tools. *Journal of Thermal Biology*, 26(4–5), 381–386. https://doi.org/10.1016/S03064565(01)00048-1.

Donnell, A. J. O., Boer, M. M., McCaw, W. L., and Grierson, P. F. (2011). Climatic anomalies drive wildfire occurrence and extent in semi-arid shrublands and woodlands of southwest Australia. *Ecosphere*, 2(11), 1-15. https://doi.org/10.1890/ES11-00189.1.

Duan, S. B., Z. L. Li, W. Zhao, P. Wu, C. Huang, and Han, X. J. (2021). Validation of Landsat Land Surface Temperature product in the conterminous United States using in situ measurements from SURFRAD, ARM, and NDBC sites. *International Journal of Digital Earth,* 14(5), 640-660. https://doi.org/10.1080/17538947.2020.1862319.

Duveiller, G., J. Hooker, and Cescatti, A. (2018). The mark of vegetation change on Earth's surface energy balance. *Nature Communications,* 9(679), 1-12. https://doi.org/10.1038/s41467-017-02810-8.

Erick, O. O., K. Kahiri, and Erick, W. M. (2017). Impact of measurement errors on estimators of parameters of a finite population with linear trend under systematic sampling. *American Journal of Theoretical and Applied Statistics,* 6(6), 270–277. https://doi.org/10.11648/j.ajtas.20170606.12.

Findell, K. L., A. Berg, J. P. Krasting, B. R. Lintner, S. Malyshev, J. A. Santanello Jr., and Shevliakova, E. (2017). The impact of anthropogenic land use and land cover change on regional climate extremes. *Nature Communications,* 8(989), 1-10. https://doi.org/10.1038/s41467-017-01038-w.

Gizachew, B., Rizzi, J., Shirima, D. D., and Zahabu, E. (2020). Deforestation and connectivity among protected areas of Tanzania. *Forests*, 11(2), 170; https://doi.org/10.3390/f11020170,

Guillevic, P., F. Göttsche, J. Nickeson, G. Hulley, D. Ghent, Y. Yu, and Trigo, I. (2018). *Land Surface Temperature product validation best practice protocol*. Version 1.1. In P. Guillevic, F. Göttsche, J. Nickeson, and M. Román (Eds.), *Good practices for satellite derived land product validation*, p.58. Land Product Validation Subgroup. https://lpvs.gsfc.nasa.gov/PDF/CEOS_LST_PROTOCOL_Feb2018_v1.1.0_light.pdf.

Gunashree, R. S. (2024). *Your comprehensive guide to mean bias*. https://www.devzery.com/post/your-comprehensive-guide-to-mean-bias?utm_source=chatgpt.com.

Gutierrez, A. A., S. Hantson, B. Langenbrunner, B. Chen, Y. Jin, M. L. Goulden, and Randerson, J. T. (2021). Wildfire response to changing daily temperature extremes in California's Sierra Nevada. *Science*

Advances, 7, eabe6417. https://pmc.ncbi.nlm.nih.gov/articles/PMC8597996/pdf/sciadv.abe6417.pdf.

Harper, A. B., T. Powell, P. M. Cox, J. House, C. Huntingford, T. M. Lenton, S. Sitch, E. Burke, S. E. Chadburn, Collins, W. J., et al. (2018). Land-use emissions play a critical role in land-based mitigation for Paris climate targets. *Nature Communications* 9(2938), 1-13. https://doi.org/10.1038/s41467-018-05340-z.

Higgins, S., W. Bond, E. February, A. Bronn, V. Euston-Brown, B. Enslin, N. Govender, L. Rademan, S. O'Regan, A. L. Potgieter, S. Scheiter, R. Sowry, L. Trollope, and Trollope, W. S. W. (2007). Effects of four decades of fire manipulation on woody vegetation structure in savanna. *Ecology,* 88(5), 1119–1125. https://doi.org/10.1890/06-1664.

Homewood, K. Sinclair A. R. E, Packer, C, S. Mduma and Fryxell, J. M. (2011). Serengeti III: Human Impacts on Ecosystem Dynamics. *Pastoralism*, 1(22), 1-6. https://doi.org/10.1186/2041-7136-1-22.

Huang, N., P. Mondal, B. I. Cook, and McDermid, S. (2021). Moisture and temperature influences on nonlinear vegetation trends in Serengeti National Park. *Environmental Research Letters,* 16(9), 094049. https://doi.org/10.1088/1748-9326/ac1a37.

IUCN [International Union for Conservation of Nature] and UNEP-WCMC [UN Environment World Conservation Monitoring Centre]. (2017). *Serengeti National Park*. http://world-heritage-datasheets.unep-wcmc.org/datasheet/output/site/serengeti-national-park/.

Jaafar, W. S. W. M., K. N. A. Maulud, A. M. M. Kamarulzaman, A. Raihan, S. M. Sah, A. Ahmad, Saad, S. N. M., Azmi, A. T. M., et al. (2020). The influence of deforestation on Land Surface Temperature – a case study of Perak and Kedah, Malaysia. *Forests,* 11(6), 670. https://doi.org/10.3390/f11060670.

Jia, L., Zu, W., Yang, F., Gao, L., Gu, G. and Zhao, M. (2023). Marine-Predators-Algorithm-Based Random Forest and Multiple Differential Transformations. *Appl. Sci*., 13(19), 10693; https://doi.org/10.3390/app131910693.

Jiang, K., Pan, Z., Pan, F., Teuling, A. J., Han, G., An, P., Chen, X., Wang, J., Song, Y *et al*., (2023). Combined influence of soil moisture and atmospheric humidity on land surface temperature under different climatic background. *iScience*, 26, 106837. https://doi.org/10.1016/j.isci.2023.106837.

Jodhani, K. H., H. Patel, U. Soni, R. Patel, B. Valodara, N. Gupta, A. Patel, and Omar, P. J. (2024). Assessment of forest fire severity and Land Surface Temperature using Google Earth Engine: A case study of Gujarat State, India. *Fire Ecology* 20(23), 1-21. https://doi.org/10.1186/s42408-024-00254-2.

Jolly, W. M., M. A. Cochrane, P. H. Freeborn, Z. A. Holden, T. J. Brown, G. J. Williamson, and Bowman, D. M. J. S. (2013). Climate-induced variations in global wildfire danger from 1979 to 2013. *Nature Communications*, 6(7537), 1-11. https://doi.org/10.1038/ncomms8537.

Joshi, R., A. Singh, T. P. Parab, J. J. Mandy, and Pande, C. B. (2024). Assessing the impact of recent climate dynamics on land since the last two decades (1991–2021) using LST and NDVI. In A. P. Mishra, A. Kaushik, and C. B. Pande (Eds.), *Natural Resource Monitoring, Planning and Management Based on Advanced Programming*. *Advances in Geographical and Environmental Sciences*. Singapore: Springer. https://doi.org/10.1007/978-981-97-2879-4_14.

Julien, Y., J. A. Sobrino, C. Mattar, A. B. Ruescas, J. C. Jiménez-Muñoz, G. Sòria, V. Hidalgo, M. Atitar, B. Franch, and Cuenca, J. (2011). Temporal analysis of Normalized Difference Vegetation Index (NDVI) and Land Surface Temperature (LST) parameters to detect changes in the Iberian land cover between 1981 and 2001. *International Journal of Remote Sensing,* 32(7), 2057–2068. https://www.uv.es/ucg/articulos/2011/Publications_2011_3.pdf.

Key, C. H. and Benson, N. C. (2006). Landscape assessment: ground measure of severity, the composite burn index; and remote sensing of severity, the Normalized Burn Ratio. In: Lutes, D. C., Keane, R. E., Caratti, J. F., Key, C. H., Benson, N.C., Sutherland, S., Gangi, L. J. (Eds *FIREMON: Fire Effects Monitoring and Inventory System*, General Technical Report (GTR). U.S. Department of Agriculture, Forest Service, Rocky Mountain Research Station, p. LA-1-55. https://purl.org/INRMM-MiD/z-B4PCNQM6.

Kideghesho, J. R. (2010). Serengeti shall not die: Transforming an ambition into a reality. *Tropical Conservation Science*, 3(3), 228–248. https://doi.org/10.1177/194008291000300301

Kija, H. K., Ogutu, J. O., Mangewa, L. J., Bukombe, J., Verones, F., Graae, B. J., Kideghesho, J. R., *et al*. (2020). Spatio-temporal changes in wildlife habitat quality in the Greater Serengeti Ecosystem. *Sustainability*, 12(6), 1-19.https://doi.org/10.3390/su12062440.

Kikon, N., D. Kumar, and Ahmed, S. A. (2023). Quantitative assessment of Land Surface Temperature and vegetation indices on a kilometer grid scale. *Environmental Science and Pollution Research International,* 30, 107236–107258. https://doi.org/10.1007/s11356-023-27418-y.

Kupfer, J. A., A. J. Terando, P. Gao, C. Teske, and Hiers, J. K. (2020). Climate change projected to reduce prescribed burning opportunities in the south-eastern United States. *International Journal of Wildland Fire,* 29(9), 764–778. https://doi.org/10.1071/WF19198.

Laris, P., Koné, M., and Dembélé, F. (2017). The early/late fire dichotomy: Time for a reassessment of Aubréville's savanna fire experiments. *Progress in Physical Geography: Earth and Environment*, 41(1), 68–94. https://doi.org/10.1177/0309133316665570.

Lee, S-H., Lee, M-H., Kang, T-H., Cho, H-R., Yun, H-S. and Lee, S-J. (2025). Comparative analysis of dNBR, dNDVI, SVM kernels, and ISODATA for wildfire-burned area mapping using Sentinel-2 imagery. *Remote Sens*., 2025, 17(13), 1-38; https://doi.org/10.3390/rs17132196.

Li, F., D. Lawrence, and Bond-Lamberty, B. (2017). Impact of fire on global Land Surface Air Temperature and energy budget for the 20th Century due to changes within ecosystems. *Environmental Research Letters* 12(4), 1-10. DOI: 10.1088/1748-9326/aa6685.

Li, Y., Y. Liu, G. Bohrer, Y. Cai, A. Wilson, T. Hu, Z. Wang, and Zhao, K. (2022). Impacts of forest loss on local climate across the conterminous United States: Evidence from satellite time-series observations. *Science of The Total Environment,* 802, 149651. https://doi.org/10.1016/j.scitotenv.2021.149651.

Li, Y., M. Zhao, D. J. Mildrexler, S. Motesharrei, Q. Mu, E. Kalnay, F. Zhao, S. Li, and Wang, K. (2016). Potential and actual impacts of deforestation and afforestation on Land Surface Temperature. *Journal of Geophysical Research: Atmospheres,* 121(24), 14,372–14,386. https://doi.org/10.1002/2016JD024969.

Liu, Z., A. P. Ballantyne, and Cooper, L. A. (2018). Increases in Land Surface Temperature in response to fire in Siberian boreal forests and their attribution to biophysical processes. *Geophysical Research Letters,* https://doi.org/10.1029/2018GL078283

Mahony, J., E. Dyer, and Washington, R. (2020). The precipitation patterns and atmospheric dynamics of the Serengeti National Park. *International Journal of Climatology,* 41(S1), E2051–E2072. https://doi.org/10.1002/joc.6831.

Masocha, M., A. K. Skidmore, Poshiwa, X., and Prins, H. H. T. (2011). Frequent burning promotes invasions of alien plants into a mesic African savanna. *Biological Invasions,* 13, 1641–1648. https://doi.org/10.1007/s10530-010-9921-6.

Muro, J., A. Strauch, S. Heinemann, S. Steinbach, F. Thonfeld, B. Waske, and Diekkrüger, B. (2018). Land Surface Temperature trends as indicator of land use changes in wetlands. *International Journal of Applied Earth Observation and Geoinformation,* 70, 62–71. https://doi.org/10.1016/j.jag.2018.02.002.

Nkwabi, A. K., & Kavana, P. Y. (2022). Vegetation and avifauna distribution in the Serengeti National Park. In *Vegetation Dynamics, Changing Ecosystems and Human Responsibility* (Environmental Sciences). IntechOpen. https://doi.org/10.5772/intechopen.106165.

Noske, P. J., P. N. J. Nyman, P. Lane, F. K. Rengers, and Sheridan, G. J. (2024). Changes in soil erosion caused by wildfire: A conceptual biogeographic model. *Geomorphology,* 459, 109272. https://doi.org/10.1016/j.geomorph.2024.109272.

Nsemwa, R. (2020). *Assessment of tourism competitive advantage of UNESCO World Heritage Sites in Tanzania: A case study of Serengeti National Park from 2000–2018*. Master's Dissertation, Open University of Tanzania. http://repository.out.ac.tz/2640/1/DISSERTATION%20%20-%20REBECA%20MAREKEBISHO-EXTERNAL%2C%2020200205.pdf.

Nyerere National Park. (2024). *Nyerere National Park*. Tanzania National Parks. https://www.nyererenationalpark.net/

Oliveira, S., Andrade, H. and Vaz, T. (2011). The cooling effect of green spaces as a contribution to the mitigation of urban heat: A case study in Lisbon. *Build. Environ*., 46(11), 2186–2194. https://doi.org/10.1016/j.buildenv.2011.04.034.

Pan, X., Z. Wang, S. Liu, Z. Yang, R. Guluzade, Y. Liu, J. Yuan, and Yang, Y. (2024). The impact of clear-sky biases of Land Surface Temperature on monthly evapotranspiration estimation. *International Journal of Applied Earth Observation and Geoinformation,* 129(103811), 1-14.https://doi.org/10.1016/j.jag.2024.103811.

Petrou, Z. I., Kosmidou, V., Manakos, I., Stathaki, T.; Adamo, M., Tarantino, C., Tomaselli, V., Blonda, P., and Petrou, M. A (2014). Rule-based

classification methodology to handle uncertainty in habitat mapping employing evidential reasoning and fuzzy logic. *Pattern Recognit. Lett.*, 48, 24–33. https://doi.org/10.1016/j.patrec.2013.11.002.

Rahimi, E., P. Dong, and Jung, C. (2025). Global NDVI-LST correlation: Temporal and spatial patterns from 2000 to 2024. *Environments* 12(2), 1-14. https://doi.org/10.3390/environments12020067.

Ren, X., Q. Zhang, P. Yue, J. Yang, and S. Wang. (2022). Environmental and biophysical effects of the Bowen Ratio over typical farmland ecosystems in the Loess plateau. *Remote Sensing* 14(8), 1-24. https://doi.org/10.3390/rs14081897.

Reeves, M. C., M. E. Manning, J. P. DiBenedetto, K. A. Palmquist, W. K. Lauenroth, J. B. Bradford, and Schlaepfer, D. R. (2018). Effects of climate change on rangeland vegetation in the Northern Rockies. In J. Halofsky and D. Peterson (Eds.), *Climate change and rocky mountain ecosystems*. Advances in Global Change Research, 63, 97–114. https://doi.org/10.1007/978-3-319-56928-4_6.

Reinsch, S., Robinson, D. A., van Soest, M. A. J., Keith, A. M., Parry, S. and Tye, A. M. (2024). Temperate Soils Exposed to Drought—Key Processes, Impacts, Indicators, and Unknowns. *Land*, 13(1759), 1-32. https://doi.org/10.3390/land13111759.

Ruckman, E. M., S. Schwinning, and Lyons, K. G. (2012). Effects of phenology at burn time on post-fire recovery in an invasive C4 grass. *Restoration Ecology* 20(6), 756–763. https://doi.org/10.1111/j.1526-100X.2011.00830.x.

Ryan, C. M., and Williams, M. (2011). How does fire intensity and frequency affect miombo woodland tree populations and biomass? *Ecological Applications* 21(1), 48–60. https://doi.org/10.1890/09-1489.1.

Sabuncu, A., and Özener. H. (2018). *Evaluating & comparing NDVI & NBR indices performance for burned areas in terms of PBIA and OBIA in Aegean Region, Turkey*. https://www.fig.net/resources/proceedings/fig_proceedings/fig2018/ppt/ts05f/TS05F_sabuncu_ozener_9387_ppt.pdf.

Sankaran, M., J. Ratnam, and Hanan, N. P. (2004). Tree-grass coexistence in savannas revisited: Insights from an examination of assumptions and mechanisms invoked in existing models. *Ecology Letters* 7, 480–490. https://doi.org/10.1111/j.1461-0248.2004.00596.x.

Schneider, P., D. Ghent, G. Corlett, F. Prata, and Remedios, J. (2012). *AATSR validation: LST validation protocol*. University of Leicester: Leicester, UK.

Schweizer, D. W., and Cisneros, R. (2017). Forest fire policy: Change conventional thinking of smoke management to prioritize long-term air quality and public health. *Air Quality, Atmosphere & Health,* 10, 33–36. https://doi.org/10.1007/s11869-016-0405-4.

Scott, A. C., D. M. J. S. Bowman, W. J. Bond, S. J. Pyne, and Alexander, M. E. (Eds.). (2014). *Fire on Earth: An introduction*. Chichester, England: John Wiley and Sons Ltd. Fire Ecology 10, 88–91. https://doi.org/10.4996/fireecology.1001088.

Shannon, C. E. and Wiener, W. (1949). *The Mathematical Theory of Communication*. Urbana, IL: University of Illinois Press.https://pure.mpg.de/rest/items/item_2383164/component/file_2383163/content

Sharashy. O. S., (2022). Plant biodiversity on coastal rocky ridges habitats with reference to census data in Ras El-Hekma and Omayed Area, Egypt. *Sebha University Journal of Pure & Applied Sciences*, 21(1), 41–45. https://doi.org/10.51984/jopas.v21i1.1578.

Sharma, B., J. Kumar, A. R. Ganguly, and Hoffman, F. M. (2023). Carbon cycle extremes accelerate weakening of the land carbon sink in the late 21st century. *Biogeosciences,* 20(10), 1829–1841. https://doi.org/10.5194/bg-20-1829-2023.

Serengeti National Park. (2024). *About Serengeti National Park*. https://www.serengeti.com/information-serengeti-national-park.php.

Serengeti National Park Safaris. (2022). *Climate and weather in Serengeti National Park*. https://serengetinationalparksafaris.com/climate-and-weather-in-serengeti-national-park/.

Serengeti National Park. (2020). *2020 Conservation outlook assessment*. https://rris.biopama.org/sites/default/files/2020-12/Serengeti%20National%20Park%20-%202020%20COA%20-%20en.pdf.

Simonetti, E., Simonetti, D., & Preatoni, D. (2014). *Phenology-based land cover classification using Landsat 8 time series*. European Commission Joint Research Centre. https://files.core.ac.uk/download/pdf/38629451.pdf. (Accessed September 11, 2025).

Sivakumar, V. L., A. Raju, and Sundaram, A. V. (2014). Study of forest fire severity through Normalized Burn Ratio analysis using Remote Sensing. *E3S Web of Conferences,* 491, 01027. https://doi.org/10.1051/e3sconf/202449101027.

Thanalapadi Sriramamurthy, R., Sankaran, M., & Bhalla, R. S. (2022). Wildfires and aliens: Differenced normalized burn ratios (dNBR) indicate that woody invasive plants increase fire intensities in montane forest–grassland mosaics of the Western Ghats, India. *Research Square*. https://doi.org/10.21203/rs.3.rs-1382178/v1

Stavi, I. (2019). Wildfires in grasslands and shrublands: A review of impacts on vegetation, soil, hydrology, and geomorphology. *Water* 11(5), 1-20. https://doi.org/10.3390/w11051042.

Strauch, A. M., and Eby S. (2021). The influence of fire frequency on the abundance of *Maerua subcordata* in the Serengeti National Park, Tanzania. *Journal of Plant Ecology*, 5(4), 400–406. https://doi.org/10.1093/jpe/rts008.

Stoyanova, J. S., C. G. Georgiev, and Neytchev, P. N. (2022). Satellite observations of fire activity in relation to biophysical forcing effect of Land Surface Temperature in Mediterranean Climate. *Remote Sensing* 14(7), 1-24. https://doi.org/10.3390/rs14071747.

Strauch, A. M., and Eby, S. (2012). The influence of fire frequency on the abundance of *Maerua subcordata* in the Serengeti National Park, Tanzania. *Journal of Plant Ecology,* 5(4), 400–406. https://doi.org/10.1093/jpe/rts008.

Szpakowski, D. M., and Jensen, J. L. R. (2019). A review of the applications of Remote Sensing in fire ecology. *Remote Sensing* 11(22), 1-31. https://doi.org/10.3390/rs11222638.

Takacs, S., H. S. to Bühne, and Pettorelli, N. (2021). What shapes fire size and spread in African savannahs? *Remote Sensing in Ecology and Conservation,* 7(4), 610–620. https://doi.org/10.1002/rse2.212.

Tiger, T. (1982). *Soils of the Serengeti Woodland*. *Agricultural Research Report*. Center for Agricultural Publishing and Documentation, Wageningen, The Netherlands. https://edepot.wur.nl/479527.

Ulfah, M., Fajri1, S. N., Nasir, M., Hamsah, K. and Purnawan, S. (2019). Diversity, evenness and dominance index reef fish in Krueng Raya Water, Aceh Besar. *IOP Conf. Ser.: Earth Environ. Sci. 348 012074*, DOI 10.1088/1755-1315/348/1/012074.

USDA [United States Department of Agriculture]. (2012). *Introduction to prescribed fire in southern ecosystems*. https://www.srs.fs.usda.gov/pubs/su/su_srs054.pdf. (Accessed October 15, 2025).

van der Walt, A., Barker, C., Kruger, E., & Kotze, N. (2018). Assessment of short-term inter-annual post-fire vegetation recovery using Land Surface Temperature (LST). In *Proceedings of the Biennial Conference of the Society of South African Geographers: 1–5 October 2018, University of the Free State* (pp. 1–X).

van Wilgen, B. W., W. S. W. Trollope, H. C. Biggs, A. L. F. Potgieter, and Brockett, B. H. (2003). Fire as a driver of ecosystem variability. In J. T. du Toit, K. H. Rogers, and H. C. Biggs (Eds.), *The Kruger Experience: Ecology and management of savanna heterogeneity*, 149–170. Washington, DC: Island Press.

Veldhuis, M. P., Ritchie, M. E., Ogutu, J. O., Morrison, T. A., Beale, C. M., Estes, A. B., Mwakilema, W., Ojwang, G. O. Parr, C.L. *et al*. (2019). Cross-boundary human impacts compromise the Serengeti-Mara ecosystem. *Science*, 363(6434), 1424–142. DOI: 10.1126/science.aav0564.

Vlassova, L., F. Pérez-Cabello, M. R. Mimbrero, R. M. Llovería, and García-Martín, A. (2014). Analysis of the relationship between Land Surface Temperature and wildfire severity in a series of Landsat images. *Remote Sensing* 6(7), 6136–6162. https://doi.org/10.3390/rs6076136.

Xie, Q., Wu, Y., Zhou, Z. & Wang, Z. (2018). Remote sensing study of the impact of vegetation on thermal environment in different contexts. IOP Conf. Series: Earth and Environmental Science, 121, 1-7, 022009. doi:10.1088/1755-1315/121/2/022009.

Yang, Y., Hsee, C. K. and Li, X. (2021). Prediction biases: An integrative review. *Current Directions in Psychological Science*, 30(3), 1–7. https://doi.org/10.1177/0963721421990341.

Zhang, Z., Pan, Z., Pan, F., Zhang, J., Han, G., Huang, N., & Wang, J. (2020). The change characteristics and interactions of soil moisture and temperature in the farmland in Wuchuan County, Inner Mongolia, China. *Atmosphere, 11*(5), 1-14. https://doi.org/10.3390/atmos11050503.

Zhao, J., L. Wang, X. Hou, G. Li, Q. Tian, E. Chan, P. Ciais, Q. Yu, and Yue, C. (2021). Fire regime impacts on post-fire diurnal Land Surface Temperature change over North American boreal forest. *Journal of Geophysical Research: Atmospheres* 126(23), (page numbers) e2021JD035589. https://doi.org/10.1029/2021JD035589.